

Dec 14 73

(12)
JK

AD A024311

Project Report

TT-7

Statistics of Global IR Atmospheric Transmission

A. P. Modica
H. Kleiman

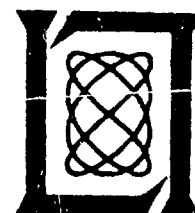
3 March 1976

Prepared for the Defense Advanced Research Projects Agency
under Electronic Systems Division Contract F19628-76-C-0002 by

Lincoln Laboratory

MASSACHUSETTS INSTITUTE OF TECHNOLOGY

LEXINGTON, MASSACHUSETTS



Approved for public release; distribution unlimited.

DDC
RECORDED
MAY 12 1976
B

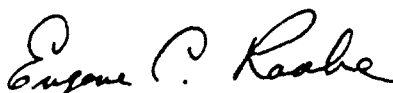
The work reported in this document was performed at Lincoln Laboratory, a center for research operated by Massachusetts Institute of Technology. This work was sponsored by the Defense Advanced Research Projects Agency under Air Force Contract F19628-76-C-0002 (ARPA Order 2752).

This report may be reproduced to satisfy needs of U.S. Government agencies.

The views and conclusions contained in this document are those of the contractor and should not be interpreted as necessarily representing the official policies, either expressed or implied, of the Defense Advanced Research Projects Agency of the United States Government.

This technical report has been reviewed and is approved for publication.

FOR THE COMMANDER

A handwritten signature in cursive script, reading "Eugene C. Raabe".

Eugene C. Raabe, Lt. Col., USAF
Chief, ESD Lincoln Laboratory Project Office

MASSACHUSETTS INSTITUTE OF TECHNOLOGY
LINCOLN LABORATORY

STATISTICS OF GLOBAL IR
ATMOSPHERIC TRANSMISSION

A. P. MODICA
H. KLEIMAN

Group 53

PROJECT REPORT TT-7

3 MARCH 1976

ADDITIONAL BY	
DTIC	White Section <input checked="" type="checkbox"/>
DOC	Patt Section <input type="checkbox"/>
UNAPPROVED	<input type="checkbox"/>
JUSTIFICATION	
BY	
DISTRIBUTION/AVAILABILITY CODES	
Doc.	DETAIL, Doc. or SPECIAL
A	

Approved for public release; distribution unlimited.

LEXINGTON

MASSACHUSETTS

ABSTRACT

RAND weather data tapes have been used to obtain statistics of visibility, relative humidity and cloud ceiling heights for a number of global weather stations to generate probabilities for atmospheric attenuation in the infrared spectral region. LOWTRAN atmospheric models for clear-air and rural fog-haze transmission have been used to correlate the observed photopic visibility (.55 - .66 μ m) and humidity to the IR attenuation. A maritime fog-haze model of Barhydt has been incorporated in the analysis to predict atmospheric attenuation losses for the 8.0 - 11.5 μ m band. Statistics for rain attenuation in the 0.6 to 10.6 μ m region were computed using the extinction data reported by Rensch and Long. The basic results of the study are global seasonal probabilities for horizontal sea level transmission losses for several narrow IR bands (1.0 - 1.2), (3.8 - 4.2), (8.0 - 11.5 μ) and four laser lines (1.06), (3.83), (4.73), and (10.6 μ m). Correction factors are provided to scale horizontal transmission losses to slant path transmittances.

CONTENTS

ABSTRACT	iii
1. Introduction	1
2. RAND Weather Data Bases	2
3. Atmospheric Transmission Models	2
3.1 Clear Air Transmission Equation	3
3.2 Fog-Haze Transmission Equation	3
3.3 Slant Path Correction Factor	7
4. Rain Attenuation	7
5. Cloud Free Line-of-Sight Probabilities	9
6. Stations Selected for IR Weather Analysis	11
7. Statistics	15
8. Weather Statistics and IR Atmospheric Attenuation Averages for Germany	16
9. Use of IR-Weather Data: Examples	19
APPENDIX	27
REFERENCES	31

PREFACE

Weather statistics are extremely important in the design of electro-optical systems for tactical operations. In the HOWLS Program, several such systems are being considered. Existing analyses and weather statistics were inadequate for effectiveness evaluations and it was necessary to initiate an effort to extrapolate available data. The present study is an attempt to correlate extensive meteorological data from a network of global weather stations sufficiently different in climatological conditions to establish a representative data base on world-wide atmospheric attenuation in the 1.0-14.0 μ m IR radiation band. Weather histories of photopic visibility and relative humidity were obtained from the RAND Weather Data Bank and were reduced to IR atmospheric propagation models. The transmission models used in the analysis are continuously being updated by current HOWLS weather measurements and through ongoing measurements programs under Project OPAQUE. The results of this work should prove valuable to many users concerned with electro-optical, global all-weather performance.

1. Introduction

Under the HOWLS Program, the analysis of FLIR imaging systems and IR sensor devices for target acquisition and PGM (precision-guided munitions) terminal guidance applications has led to the need to assess the impact of weather statistics and atmospheric attenuation in the infrared on the effectiveness of such types of tactical weapon systems. The primary objective of IR-weather analysis is to collate meteorological data for a number of worldwide weather stations and to determine the extent and frequencies of IR attenuation losses extrapolated from photopic visibilities and relative humidity measurements. RAND Weather Tapes¹ have been processed by a computer to determine the seasonal and geographical variations of these weather parameters for a number of selected Northern Hemisphere weather stations: Berlin, Dresden, Essen, and Hamburg in Germany; Nicosia, Cyprus; Cairo, Egypt; Hue, South Vietnam; Hanoi, North Vietnam; and Falmouth, MA, USA. These statistics and the AFCRL LOWTRAN atmospheric models for clear air and fog-haze transmission² have been correlated to generate probability curves for horizontal sea level atmospheric attenuation losses for three narrow IR radiation bands (1.0-1.2), (3.8-4.2), (8.0-11.5 μ m) and four laser lines (1.06), (3.83), (4.73), (10.6 μ m). Joint probabilities of transmission losses with cloud ceiling height have also been computed and indicate the seasonal and worldwide variability. Synoptic weather statistics for precipitation, cloud ceiling heights and photopic visibilities have been included for examination to demonstrate similarities and differences in weather between the various geographical locations.

2. RAND Weather Data Bases

Weather data have been compiled by the RAND Corporation¹ for a network of global weather stations and are available on 9 track, 1600 bpi density magnetic tapes. The data bank of each weather station is a chronology of atmospheric variables including the parameters of dew point temperature (relative humidity), photopic visibility, weather conditions (rain, fog, haze, drizzle, etc.) and cloud data (cloud amounts, ceiling heights). The principle source of the RAND Weather Data Bank (RAWDAB) is derived from weather observation records collected by the USAF Environmental Technical Applications Center³. The RAWDAB tapes are written in EBCDIC Code having a physical record block of 50 logical records, 96 characters in length. Groups of weather stations in close proximity were chosen to compare similarities in local weather conditions. Sufficient groups were chosen with widely varying weather patterns to provide a representative global weather data base.

3. Atmospheric Transmission Models

In the present study, the atmospheric attenuation of radiation in the 1.0-14.0 μ m infrared region is of primary interest. Models for atmospheric transmission in the IR deal primarily with molecular absorption by atmospheric CO₂ and water vapor gases, and with the scattering of radiation by various types of aerosols (rural, continental, maritime), whose normalized extinction coefficients are shown for comparison in Figure 1. The AFCRL LOWTRAN computer program² has been used to compute atmospheric transmittances

for three narrow IR radiation bands (1.0-1.2), (3.8-4.2), and the (8.0-11.5 μ m) thermal band for horizontal sea level paths. The LOWTRAN code was run for a sequence of relative humidities and visibility ranges with the resultant transmittances being fitted to exponential laws of the form⁴:

3.1 Clear Air Transmission Equation

$$T_A = \exp [-R(A/W + B)] \quad (1)$$

and

3.2 Fog-Haze Transmission Equation

$$T_F = \exp [-R(A/V^C)] \quad (2)$$

where R is the optical path length, km, W is the amount of H₂O absorber, ft per mm of precipitable H₂O (Ft/mm-prec H₂O), V is the photopic visibility range, km, and A, B, and C are the coefficients derived from a three-point average curve fit. The amount of water vapor absorber in ft/mm-prec H₂O is given in terms of the percent relative humidity, RH, and the air temperature, TK ($^{\circ}$ K,) by⁵

$$W = 3.3(10^5) / \left[RH \left(\frac{TK}{247} \right)^{16.8} - .616RH \right] \quad (3)$$

or in terms of the H₂O partial pressure⁶, P_{H₂O}

$$W = 0.114(10^2) TK/P_{H_2O} \quad (4)$$

Similar clear air and fog-haze transmission expressions were derived for four IR laser lines using spectral absorption and extinction coefficients obtained from AFCRL⁷. Barhydt's maritime fog-haze model⁵ was used as a lower bound to the LOWTRAN rural aerosol model for the (8.0-11.5 μ m) band. Clear air transmission for the 10.6 μ m laser line was calculated with the expression given by Long, et al, in a study of water vapor continuum absorption of CO₂ laser radiation near 10 μ m⁶. A comparison of Barhydt's and Long's transmission curves with the LOWTRAN Model is shown in Figure 2. Figure 3 shows the clear air and fog-haze transmission curves for the IR radiation bands calculated with the LOWTRAN code. A summary of the atmospheric clear air and fog-haze transmission models used in the meteorology statistical analysis is given in Table 1. The difference in the transmission equations for the bands and lines reflects the fact that the band coefficients are related to vibrational-rotational line spectral absorption and extinction factors integrated over the bandwidth. Based on the work of Eldridge⁸, the fog-haze atmospheric boundary occurs abruptly and represents a transition at about a 1.2 km visibility. Hulbert⁹ has found that the haze-clear boundary condition is more diffusive, approximately a 15 km visibility range. Table 2 catalogs the different types of fogs according to their photopic visibilities and compares the attenuation loss performances for the (3.8-4.2) and (8.0-11.5 μ m) bands, and the 1.06 and 10.6 μ m laser lines.

TABLE 1

IR NARROW BAND AND LASER LINE ATMOSPHERIC
TRANSMISSION EQUATIONS

Narrow Band Atmospheric Transmission in the Infrared

Radiation:	<u>Clear Air Transmission</u>	<u>Fog Haze Transmission</u>
^a (1-1.2) μm	$T_W = \exp \{-R[35.9/(W) + .065]\}$	$T_F = \exp \{-2.02R/(V)^{.997}\}$
(3.8-4.2) μm	$T_W = \exp \{-R[10.47/(W) + .098]\}$	$T_F = \exp \{-.796R/(V)^{.855}\}$
^b (8-11.5) μm	$T_W = \exp \{R[.987/(W)^{.384}$ $+ 5930/(W)^{1.86}]\}$	$T_F = \exp \{-0.8R/(V)^{1.26}\}$

a. Ref. 2, b. Ref. 5

Laser Line Atmospheric Transmission in the Infrared

Radiation:	^a <u>Clear Air Transmission</u>	^a <u>Fog-Haze Transmission</u>
(1.06) μm	$T_W = \exp \{-0. R/w\}$	$T_F = \exp \{-2.20R/(V)\}$
(3.83) μm	$T_W = \exp \{-R(.002078 + 1.937/w)\}$	$T_F = \exp \{-.526R/(V)\}$
(4.73) μm	$T_W = \exp \{-R(.0013 + 16.366/w)\}$	$T_F = \exp \{-.44R/(V)\}$
(10.6) μm	^b $T_W = \exp \{-R [144.(295./TK)^{1.5}$ $(10)^{-970/TK} + .0374 (TK/W)$ $+ .1078 (TK/W)^2]\}$	$T_F = \exp \{-.391R/(V)\}$

Units, W(FT/MM - prec H₂O, V(KM), R(KM), TK(°K)

a. Ref. 7, b. Ref. 6

TABLE 2

COMPARISON OF FOG-HAZE VISIBLE/INFRARED
ATMOSPHERIC TRANSMITTANCES

*TYPE	H ₂ O CONTENT (G/M ³)	VISIB (KM)	IR BANDS μ M		LASER LINE μ M	
			DB KM ⁻¹ (3.8-4.2)	(8-11.5)	DB KM ⁻¹ 10.6	1.06
THICK	0.4	.03	69.9	45.3	58.1	318.4
MEDIUM	.16	.085	28.9	17.7	21.4	112.4
LIGHT	.063	.170	16.4	10.1	11.5	56.2
MIST	.027	.30	10.3	6.6	7.2	31.8
HAZE	.005	1.0	4.1	3.2	3.2	9.6

* Inland Fog @ 70°, 90% relative humidity

LOWTRAN rural fog-haze model

The slant path correction factor Δ is used to convert sea level horizontal attenuation losses to slant path attenuation losses and is given by the expression.⁶

3.3 Slant Path Correction Factor

$$\Delta = L^{-1} \csc \phi \int_0^L e^{-\frac{h}{\Delta H_0}} dh \quad (5)$$

where $e^{-\frac{h}{\Delta H_0}}$ is the geometric mean vertical scale factor for the water

vapor number density and aerosol particle number density, L is the slant path range, km, h is the vertical height, and ϕ is the elevation angle. Equation 5 was evaluated using the vertical scale normalized distributions shown in Table 3. Values of the slant path correction factors are given in Figure 4 for slant angles between 0 and 90° elevation and slant ranges from 0.5 to 10 km. The geometric mean slant path correction factors are used for atmospheres having 2 km to 10 km visibilities. Limiting exact solutions for scaling sea level horizontal attenuation losses to slant path losses are obtained by using the exact aerosol or water vapor slant path correction factor for atmospheric visibilities < 2 km and > 10 km, respectively.

4. Rain Attenuation

In the visible and IR spectral region, attenuation by rain is expected to be independent of wavelength because the raindrop radius (typically, about 0.5 cm) is much larger than the wavelength where the Mie extinction efficiency factor asymptotically approaches the value 2. Measured values of the

TABLE 3

NORMALIZED VERTICAL SCALE FACTORS FOR ATMOSPHERIC WATER
VAPOR AND AEROSOL DISTRIBUTIONS

	$Z(h) = N(h)/N_0$										
(KM)	0	1	2	3	4	5	6	7	8	9	10
1 WATER VAP	1.0	.71	.51	.34	.19	.109	.06	.024	.01	.0046	.0039
2 AEROSOL	1.0	.37	.13	.049	.018	.0055	.0046	.0042	.0044	.0042	.0041
3 GEOM. MEAN	1.0	.51	.26	.129	.058	.027	.017	.010	.0066	.0044	.004

1. Handbook of Geophysics and Space Environment (1965)

2. Elterman, L., Appl. Opt. 9, 1804 (1970)

3. Geom. Mean = $\left[Z(h)_{H_2O} \cdot Z(h)_{AERO} \right]^{1/2}$

visible and IR extinction coefficients through rain are found to compare favorably with theoretical prediction¹⁰ as shown in Figure 5. These rain attenuation results and the LOWTRAN clear air transmission models were used to reduce meteorological relative humidity and visibility data to IR attenuation losses through rain.

5. Cloud Free Line-of-Sight Probabilities

The cloud free line-of-sight (CFLOS) probability is another important weather parameter used in optical-systems analysis and is defined as the frequency of time an observer will find a line-of-sight unobstructed by clouds along a viewing angle from ground level to a given point above ground. RAND meteorological data have been queried to obtain seasonal (CFLOS) statistics as a function of viewing angle, α and line-of-sight from ground level to points, h in space. The CFLOS probabilities are computed from the equation

$$P_{CFLOS} = \sum_{k=0}^8 c(\alpha, k) \cdot D(h, k), \quad (6)$$

where $D(h, k)$ is the cumulative probability that the cloud cover in eights, k (Octas sky cover) will be equal to or less than a given height, and $c(\alpha, k)$ is the clear view function (Table 4) related to the probability that a cloud free line-of-sight will exist through cloud cover at or below the viewing point along the viewing angle¹¹. CFLOS probabilities have been determined from available cloud data for Berlin, Essen, Hamburg, Nicosia, Cairo, Hue and Falmouth USA representing the HOWLS weather data base. These

TABLE 4

CLOUD COVER CLEAR VIEW PROBABILITY FUNCTION

CLOUD COVER(EIGHTS)	ELEVATION ANGLE(DEG)															
	0.0	5.0	10.0	15.0	20.0	25.0	30.0	35.0	40.0	45.0	50.0	55.0	60.0	65.0	70.0	75.0
	PROBABILITY															
0	.962	.965	.970	.973	.975	.978	.980	.983	.985	.988	.990	.993	.995	.995	1.000	1.000
1	.640	.730	.820	.875	.895	.910	.920	.930	.940	.945	.950	.952	.954	.954	0.960	0.960
2	.490	.600	.695	.753	.805	.825	.850	.860	.875	.880	.890	.895	.898	.898	0.900	0.900
3	.370	.490	.590	.645	.700	.730	.775	.790	.800	.815	.825	.830	.840	.840	0.850	0.850
4	.275	.320	.425	.540	.600	.645	.680	.695	.710	.725	.740	.750	.765	.765	0.780	0.780
5	.195	.280	.360	.420	.490	.525	.575	.595	.610	.630	.650	.660	.675	.675	0.680	0.680
6	.095	.180	.250	.300	.365	.400	.430	.460	.480	.500	.510	.520	.525	.525	0.545	0.545
7	.040	.090	.130	.190	.225	.250	.275	.290	.300	.320	.325	.330	.340	.340	0.350	0.350
8	.020	.025	.030	.035	.040	.045	.050	.055	.060	.065	.070	.075	.080	.080	0.085	0.085

results are given in Table A-2 of the appendix for viewing angles of 1, 2, 3, 5, 15, 45, 90 degree-elevation and line-of-sight paths from ground to .333, .5, 1. and 2 km cloud heights.

6. Stations Selected for IR Weather Analysis

The RAND Weather Data Bank (RAWDAB) was used in the present study to provide visibility, relative humidity, cloud ceiling heights and synoptic weather parameters for four typical regions of the Northern Hemisphere; Europe, North Africa, Southeast Asia and Eastern USA. A general meteorological description of each geographic area is given below as summarized by Rosen and Schutz.¹¹

Europe: (Berlin, Essen, Dresden, Hamburg)

These weather stations lie in the rolling hills of northern German plains and come under the influence of a prevailing westerly flow of moist polar air generated in the North Atlantic high. There is extensive cloudiness throughout the year and little regional variation in climate. In winter, the moist Atlantic polar air becomes cool and stabilizes, resulting in persistent low broken-to-overcast stratus or strato-cumulus cloud cover. In summer, the highest cloud amounts occur during the day, since the land is warmer than the surrounding ocean creating unstable convective currents in the moist polar air mass. Overcast conditions are half that of winter, although the frequency of broken cloud cover remains about the same. Cumulus and cumulonimbus clouds (rain clouds) tend to dominate. The frequency of this cumulonimbus activity takes place on the average 4 to

6 days per month. These line squalls are similar to those experienced across the eastern United States, but are less violent because the polar air masses tend to be less moist than the tropical air masses influencing eastern United States.

North Africa: (Nicosia and Cairo)

These weather stations lie on the coastal reaches of the eastern Mediterranean, and come under the influence of the Atlantic polar air mass moving clockwise around the North Atlantic high. Expansion and compression of this air mass while crossing the east-west mountain chain of western Europe causes a loss in moisture. Before reaching the Nicosia and Cairo areas, however, some moisture is again added to the lower levels by passage over the warm Mediterranean. This added moisture accounts for the high percentage of scattered to broken clouds annually. Characteristically, Cairo and the eastern Mediterranean coast are wet in winter and dry in summer. In winter, storms intensify over the eastern portion of the polar front in the vicinity of Cyprus on an average of 4 to 6 times per month and account for the high percentage of broken-to-overcast cloud layers. In summer, low strato-cumulus clouds move inland as the land cools in the late afternoon. They remain through the night and then dissipate or form small cumulus clouds by late morning as the land becomes warmer. During the early morning period to early evening, the cloud cover increases rapidly between 2 and 4000 ft then remains constant. The low stratus or cumulus-type clouds provide the only obscuration of the ground from all levels

above. Weak upper-level disturbances occasionally pass the eastern Mediterranean area but have little or no effect on the cloud pattern below 16,000 ft.

Southeast Asia: (Hue, Hanoi)

Vietnam and the remaining peninsula of Southeast Asia come under the influence of two major monsoonal flows. From May to September, the southwest monsoon brings dried tropical ocean air to the Hue area. In October a shift begins, so that from November to March the northeast monsoon prevails, sending moist polar continental air into Hue and the surrounding coast. These area masses are somewhat similar to those that influence the area south and east of the Great Lakes. Winter conditions at Hue and along the coastal slopes of the Annam Range (from about 12°N latitude to the Red River delta) give broken-to-overcast low clouds approximately 70 percent of the time. This results from dry stable polar continental northeast flow over the Gulf of Tonkin and the South China Sea and accounts for the sharp increase below 6000 ft of persistent low stratus and strato-cumulus weather. From May to September, the period of the southwest monsoon, cloudiness during the daytime (0600 to 1800 LST) decreases caused by a drying of the unstable tropical ocean air through an adiabatic cooling and heating process as the air mass moves across the Annam Range from the southwest. Cloud cover is predominantly scattered-to-broken cumulus-type clouds with base heights around 2500 ft.

Eastern United States: (Falmouth)

The east coast region of the United States comes under the influence of the continental polar air mass in winter and a tropical ocean air mass in summer. In winter, the eastern United States has clear weather about 8 percent of the time and has only 10 percent scattered cloudiness. The Gulf Stream which carries moist tropical ocean air along a frontal path extending to the western coast of Europe (England) is modified by the cooler polar North Atlantic high, creating infrequent extended periods of fog for this area. In winter, the same Gulf Stream is turned westward by this polar Canadian high creating similar fog conditions along the eastern border of the United States. Winter fogs in western Europe are similar to those of eastern United States, both regions being fed by the same moist tropical air masses. Summer weather is less complicated by extensive storms, although line squalls in late spring and early fall sometimes prevail. The predominant cloud is cumulus within the dominating moist, unstable Atlantic air mass.

Of the stations considered in this study, from an annual viewpoint, Eastern United States and Europe represent the cloudiest stations. Hue or Southeast Asia is next in amount of cloud-cover and the Cairo area, being represented by a relatively dry polar air mass, has a minimum of cloud cover. The information provided by these global weather areas represents in this report a broad sample of the kind of climatic variation suitable to form the basis for a statistical analysis applicable to atmospheric IR attenuation losses on a worldwide scale.

7. Statistics

Some meteorological data for certain weather stations were not available on the RAWDAB tapes for statistical analysis. It was found for example that the Berlin and Falmouth tapes did not contain records on synoptic weather conditions. Also, the Dresden and Hanoi tapes did not have data on cloud ceiling heights. For clarification, a definition of the statistical quantities used in the analysis will be briefly discussed here.

Frequency of occurrence: the fraction of time a statistical parameter is recorded within a given data group.

Synoptic probability: the frequency of occurrence of a given weather condition, i.e., rain, fog, haze, fraction of cloud cover.

Seasonal probability: frequency of occurrence during winter, DEC. JAN. FEB.; Spring, MAR. APL. MAY; summer, JUN. JUL. AUG.; and fall, SEPT. OCT. NOV.

Atmospheric attenuation probability: the integrated frequency of occurrence where the meteorological parameter is equal to or greater than its value (independent of cloud ceiling height).

Joint probability of cloud ceiling height and atmospheric attenuation: probability that the attenuation is equal to or greater than its value and the cloud ceiling height is equal to or below the indicated cloud height.

Cloud ceiling height probability: defines the integrated frequency of occurrence of the cloud height being equal to or below the indicated value.

Photopic visual probability: defines the integrated frequency of occurrence of the (.5 - .6 μ m) visual range being equal to or less than the indicated value.

Attenuation losses of selected narrow band and laser line transmittances in the 1.0-14.0 μ m IR region were calculated from relative humidity and photopic visibilities, using clear air and rural fog-haze expressions given by the AFCRL LOWTRAN atmospheric models. The LOWTRAN models for rural, continental and urban aerosols show relatively small differences in their normalized extinction coefficients for the 1.0-14.0 μ m spectral region, thereby making the present analysis less sensitive to the types of inland fogs and almost completely general for correlation with photopic visibilities. For the 8.0-11.5 μ m band, atmospheric attenuation losses were computed with the maritime fog-haze transmission model of Barhydt.

8. Weather Statistics and IR Atmospheric Attenuation Averages for Germany

Synoptic weather, photopic visibility and cloud ceiling height: The synoptic weather averages for Germany (Figure 6) show that the frequency of occurrence of clear days during the year varies from about 55 percent of the time in winter and increases to about 70 percent of the time for summer. The second dominant weather condition is rain, occurring about 25-30 percent of the time throughout the year. The occurrence of fog appears to be greater in winter and fall, but slightly less in spring and summer and averages between 5 and 10 percent of the total weather events. The standard deviations from the mean values suggest that for Germany or European weather

there is little regional variation in climate throughout the year, in agreement with the meteorological description of Rosen and Schutz.

Average meteorological visibilities for Germany (Figure 7) show that visibilities equal to or less than 10 km occur about 80 percent of the time in winter and about 40 percent of the time in summer. Poor weather, where visibilities are equal to 1 km and less, appears to take place with a frequency between 5 and 10 percent throughout the four seasons and tends to correlate well with the synoptic weather data for fog and haze frequencies. Plots of short-term (6-hour time intervals) visibility data for three European cities; Leipzig, Dresden, and Prague (Oct. 10-30, 1960) are shown in Figure 8. These data have been cross-correlated¹², also, to show the degree of temporal similarities in visibility for typical European weather.

Cloud ceiling height averages (Figure 9) show that base heights equal to or below 1 km occur between 60 and 80 percent of the time for winter, spring, and fall. In summer, base heights that are equal to 1 km and below occur about 55 percent of the time, again reflecting the year round cloudy characteristics of European weather. Figure 10 shows that the short-term variability of cloud ceiling height for Leipzig, Dresden and Prague. The almost complete correlation in cloud heights for these three weather zones indicates that cloud cover extends uniformly over large distances in Europe.

IR atmospheric attenuation loss averages: Average IR attenuation losses for Germany were computed for the three narrow band wavelengths, (1.0-1.2), (3.8-4.2), and (8.0-11.5) μm shown in Figure 11. The error bars

in the figure indicate typically about a 10 percent standard deviation from the mean values calculated from the Berlin, Dresden, Essen and Hamburg weather data. The results show that for the (8.0-11.5) μm band, the attenuation loss in winter for clear and fog-haze weather conditions is equal to or more than 1.5-1.75 dB/km about 10-5 percent of the time, respectively. In summer, the (3.8-4.2) μm band shows about the same statistics on the average. The reason for the high performance of the (8.0-11.5) μm band in winter and the high performance of the (3.8-4.2) μm band in summer is accounted for by the low relative humidity in winter, since the (8.0-11.5) μm band is more sensitive to water vapor absorption and less sensitive to fog-haze scattering. The (3.8-4.2) μm band is better in summer, since this spectral band is less sensitive to water vapor absorption or high relative humidity and only moderately affected by fog-haze conditions. The (1.0-1.2) μm band which is most sensitive to aerosol scattering gives attenuation losses about a factor of two greater for the same frequency of occurrence.

Rain attenuation loss averages: The average frequency for rain attenuation losses in Germany is shown in Figure 12. The attenuation losses were calculated for the (1.0-1.2), (3.8-4.2), (8.0-11.5) μm IR bands and the visible wavelength interval (.5 - .6) μm . These calculations included clear-air water vapor absorption and losses due to rain drop scattering and liquid absorption. These data show little variation in attenuation losses for the IR-bands and the visible region, indicating that the attenuation loss here is dominated by rain scattering and absorption and less by clear-air water vapor absorption. The results show that for

Germany, about 50 percent of the time, the atmospheric losses on the average can be expected to be equal to or greater than 3 dB/km in rain.

Figure 13 is shown to compare the probability of atmospheric attenuation losses for clear weather, fog-haze and rain atmospheric conditions. This figure also shows rain rates correlated to attenuation losses for the visible (.5 - .6) μ m band. The results indicate clearly the advantages of the IR bands for fog-haze transmission over the visible band. It is also noticed that in the visible, attenuation losses are greater in fog than in rain all of the time. In the infrared, attenuation losses less than 2 dB/km occur in fog between 20 and 35 percent of the time. These conditions never exist in the rain.

Attenuation due to rain is always greater than 2 dB/km, with 50 percent of the rain having attenuation between 2 and 3 dB/km. However, for infrared attenuation above 3 dB/km, an inversion takes place between rain and fog transmission, where attenuation losses equal to or less than 3 dB/km occur more frequently in rain than during foggy conditions.

9. Use of IR-Weather Data: Examples

Weather statistics and probabilities for IR and visible attenuation losses are compiled in the Appendix according to the weather stations studied in this report. A number of examples are treated here to illustrate the use of these figures.

- Synoptic Weather Statistics (Figures A*.1)

These figures provide the fraction of time during the four seasons

that clear weather, haze, fog, drizzle and rain occur, respectively.

- Probability of Cloud Ceiling Height (Figures A*.2)

These figures give the cumulative probability, $P_{CH}(h)$, that a cloud base will be equal to or less than a given altitude, h . The cumulative probability that a cloud base will be equal to or greater than this altitude is

$$P_{CH} = 1 - P_{CH}(h).$$

The probability, $P_{CH}(S)$, that a cloud base will occur at or below a slant range, L and elevation angle ϕ is

$$P_{CH}(S) = P_{CH}(H),$$

where $H = L \sin \phi$, the terminal altitude of the slant path.

- Probability of Photopic Visibility (Figures A*.3)

These figures give the cumulative probability, $P_{vis}(v)_0$, that the horizontal sea level visibility will be equal to or less than a given meteorological range, v . The probability that the visibility will be equal to or greater than this range is

$$P_{vis} = 1 - P_{vis}(v)_0.$$

The probability, $P_{vis}(V)_s$, that the visibility along a slant path, $(V)_s$ of range, L and slant angle, ϕ is equal to or less than a given value is the probability along an equivalent horizontal sea level visibility path, $(V)_0$, i.e.,

$$P(V)_s = P(V)_o$$

where

$$(V)_o = (V)_s \times \Delta_{aero}^{\sim}$$

and Δ^{\sim} is the slant path correction factor for a slant range, L and angle, ϕ (Figure 4).

- Probability of Atmospheric Attenuation (Figures A*.4 and A*.5 bands and laser lines)

These figures give the cumulative probability, $P_a(\beta_\lambda)_o$ that the horizontal sea level attenuation loss is equal to or greater than a given value, β_λ for a particular band or laser line (λ). The probability that the attenuation loss is equal to or less than this value is

$$P_a = 1 - P_a(\beta_\lambda)_o.$$

The probability, $P_a(\beta_\lambda)_s$ along a slant path of range, L and slant angle ϕ is

$$P_a(\beta_\lambda)_s = P_a(\beta_\lambda)_o$$

where $(\beta_\lambda)_o$ is the equivalent sea level attenuation loss

$$(\beta_\lambda)_o = (\beta_\lambda)_s \times \Delta^{\sim-1}$$

and Δ^{\sim} is the corresponding slant path correction factor. The joint probability $P_a^{\lambda_1\lambda_2}$, that the attenuation loss is equal to or greater than a given value is

$$P_a^{\lambda_1\lambda_2} = P_a(\beta_{\lambda_1})_o \cdot P_a(\beta_{\lambda_2})_o$$

for a horizontal sea level path and two wavelength intervals λ_1 and λ_2 . The corresponding probability for the attenuation loss to be equal to or less than a certain value is

$$P_a^{\lambda_1 \lambda_2} = \left[1 - P_a(\beta_{\lambda_1})_0 \right] \left[1 - P_a(\beta_{\lambda_2})_0 \right]$$

For slant path joint probabilities the equations are

$$P_a^{\lambda_1 \lambda_2}(s) = P_a(\beta_{\lambda_1})_s \cdot P_a(\beta_{\lambda_2})_s \equiv P_a(\beta_{\lambda_1})_0 \cdot P_a(\beta_{\lambda_2})_0$$

where

$$(\beta_{\lambda_n})_0 = (\beta_{\lambda_n})_s \times \Delta^{-1}$$

and n is either λ_1 or λ_2 .

- Joint Probability of Cloud Height/Atmospheric Attenuation (Figures A*.6 and A*.7 IR Bands and Laser Lines)

These figures give the joint probability $P_{CH,a}$, that the horizontal sea level attenuation loss $(\beta_{\lambda})_{0,CH}$ for a band or laser line will be equal to or greater than a given value for cloud ceiling heights equal to or less than a given altitude. The slant path probability that the attenuation loss along the path is equal to or greater than a given value for a cloud ceiling height equal to or less than a given altitude is

$$P_{CH,a}(\beta_{\lambda})_{s,CH} = P_{CH,a}(\beta_{\lambda})_{0,CH}$$

where

$$(\beta_{\lambda})_{0,CH} = (\beta_{\lambda})_{s,CH} \cdot \Delta_{s,CH}^{-1}$$

and $\Delta_{s,CH}^{\sim}$ is the slant path correction factor evaluated for a slant range L , and slant angle $\phi = \arcsin \left(\frac{h}{L} \right)$. The conditional probability that the slant path attenuation loss for two wavelengths be equal to or greater than a given dB loss becomes

$$P_{CH,a_s}^{\lambda_1 \lambda_2} = P_{CH,a}(\beta_{\lambda_1})_s \cdot P_{CH,a}(\beta_{\lambda_2})_s.$$

The probability that the slant path attenuation loss for two wavelengths be equal to or less than a given dB loss is

$$P_{CH,a_s}^{\lambda_1 \lambda_2} = \left[1 - P_{CH,a}(\beta_{\lambda_1})_s \right] \left[1 - P_{CH,a}(\beta_{\lambda_2})_s \right]$$

The conditional probability that the cloud ceiling height be equal to or greater than a given altitude, and the slant path attenuation for two wavelengths be equal to or less than a given dB loss is

$$P_{CH,a_s}^{\lambda_1 \lambda_2} = \left[1 - P_{CH}(h) \right] \cdot P_{CH,a_s}^{\lambda_1 \lambda_2}$$

- HOWLS Application of These Data: Examples

1. Calculate for a 2-color IR passive homing sensor the probability that the cloud ceiling height will be equal to or greater than .33 km altitude along a 3 km slant path where the attenuation loss for both the (3.8 - 4.2) μ m band and the (8.0 - 11.5) μ m band is less than or equal to 10 dB for winter (Hamburg, Germany, data). From Figure A4.2, the probability for the cloud height to be equal to or greater than .33 km is

$$P_{CH} = 1 - P_{CH}(1) = 0.92$$

The slant angle, ϕ is

$$\phi = \arcsin \left(\frac{.33}{3} \right) = 6^\circ$$

The slant path correction factor Δ_{geom}^{\sim} for a slant range of 3 km and 6° slant angle is (Figure 4)

$$\Delta_{geom}^{\sim} = 0.8$$

The equivalent horizontal sea level attenuation loss for the (3.8 - 4.2) μ m and (8.0 - 11.5) μ m bands are

$$(\beta_{3.5})_0 = (\beta_{8.0})_0 = (3.3) / .8 \approx 4 \text{ dB/km.}$$

The corresponding probabilities that the attenuation loss will be equal to or greater than 4 dB/km for cloud ceiling heights equal to or below .33 km (Figure A4.6) are

$$\frac{(3.8-4.2)\mu\text{m band}}{P_{CH,a} (.33_{3.8})_{0,1}} = .07$$

$$\frac{(8.0-11.5)\mu\text{m band}}{P_{CH,a} (.33_{8.0})_{0,1}} = .05$$

The conditional probability that the cloud ceiling height be equal to or greater than .33 km, and the 3 km slant path attenuation for the two wavelengths be equal to or less than 10 dB loss is

$$P_{CH,a_s}^{\lambda_1 \lambda_2} = [.92][1 - .07][1 - .05] \cong .81$$

i.e., about 80 percent of the time this conditional probability will occur.

2. Calculate for the IR Countermortar System the joint probability as a function of slant angles (1° , 2° , 3°) that the cloud ceiling will be equal to or greater than the terminal altitude for the slant range of 5 km and a transmittance equal to or less than 12 dB in attenuation losses for the (8.0-11.5) μ m band in winter (Hamburg, Germany, data). Using the same procedure as in the previous example, the results of this problem are given in Table 5. It is seen in this case, that the system will work about 40 percent of the time in winter for a slant stare-angle of 3° , and that the systems utility is increased to about 60 percent of the time for a stare-angle of 1° .

TABLE 5
RESULTS OF A JOINT PROBABILITY PROBLEM

CASE I
RADIATION: (8.0-11.5) μ m Band
ATTENUATION LOSS: 12 db Winter (Hamburg, Germany)
SLANT RANGE: 5km

Slant Angle ($^{\circ}$)	Cloud Height (km)	χ_{GEOM}	$(\beta_{8.0})_s$	$\frac{db}{km}$	$(\beta_{8.0})_o$	$\frac{db}{km}$	$P_{CH}(H)$	$P_{CH,a}(\beta_{8.0})_{o,CH}$
1.0	.087	.94	2.4	2.55	.1	.32		
2.0	.174	.93	2.4	2.58	.25	.30		
3.0	.262	.92	2.4	2.60	.40	.28		

JOINT PROBABILITIES FOR CASE I

Slant χ ($^{\circ}$)	$1-P_{CH}$	$1-P_{CH,a}(\beta_{8.0})_{o,CH}$
1.0	.61	
2.0	.53	
3.0	.43	

APPENDIX

The appendix contains the detailed results for each of the stations used in this work. Seven sets of plots (where data were available) are given for each location, as follows:

- Probability of Synoptic Weather (for each season)
- Probability of Cloud Ceiling Height
- Probability of Photopic Visibilities
- Probability of Atmospheric Attenuation for IR Bands (for each of 8.0-11.5, 3.8-4.2, and 1.0-1.2 μ m bands)
- Probability of Atmospheric Attenuation for IR Lines (for each of 10.6, 4.73, 3.8, and 1.06 μ m laser lines)
- Joint Probability of Cloud Heights and Atmospheric Attenuation for IR Bands (for each of three bands and altitudes of 0.33, 0.5, 1.0, and 2.0 km)
- Joint Probability of Cloud Height and Atmospheric Attenuation for IR Lines (for each four lines and four altitudes)

Probability curves are given for each of the nine stations listed below.

Berlin, Germany	(52°-28'N, 13°-24'E)
Dresden, E. Germany	(51°-08'N, 13°-46'E)
Essen, Germany	(51°-24'N, 6°-58'E)
Hamburg, Germany	(53°-38'N, 9°-59'E)
Cairo, Egypt	(30°-8'N, 31°-34'E)
Nicosia, Cyprus	(35°-9'N, 33°-17'E)
Hue, S. Vietnam	(16°-24'N, 107°-51'E)

Hanoi, N. Vietnam ($21^{\circ}-1'N$, $105^{\circ}-51'E$)

Falmouth, Mass. USA ($41^{\circ}-39'N$, $70^{\circ}-31'W$)

Table A-1 indicates the figure number which presents each of these sets of data.

Table A-2 gives seasonal cloud free line-of-sight statistics as a function of viewing angle and line-of-sight path above ground for the same geographic area.

TABLE A-1
FIGURES IN APPENDIX PRESENTING STATISTICAL
WEATHER AND ATMOSPHERIC ATTENUATION

	Berlin	Dresden	Essen	Hamburg	Cairo	Nicosia	Hue	Hanoi	Falmouth
Prob. Synoptic Weather	----	A2.1	A3.1	A4.1	A5.1	A6.1	A7.1	A8.1	----
Prob. Cloud Ceiling	A1.2	----	A3.2	A4.2	A5.2	A6.2	A7.2	----	A9.2
Prob. Photopic Visibility	A1.3	A2.3	A3.3	A4.3	A5.3	A6.3	A7.3	A8.3	A9.3
Prob. Atmo. Atten. IR Bands	A1.4	A2.4	A3.4	A4.4	A5.4	A6.4	A7.4	A8.4	A9.4
Prob. Atmo. Atten. IR Laser Lines	A1.5	A2.5	A3.5	A4.5	A5.5	A6.5	A7.5	A8.5	A9.5
Joint Prob. Cloud/Atmo. Atten. IR Bands	A1.6	****	A3.6	A4.6	****	A6.6	****	****	A9.6
Joint Prob. Cloud/Atmo. Atten. IR Laser Lines	A1.7	****	A3.7	A4.7	****	A6.7	****	****	A9.7

**** Joint meteorological data not available

---- Meteorological data not available

TABLE A-2

GLOBAL CLOUD FREE LINE-OF-SIGHT STATISTICS

BERLIN, GERMANY
DAYTIME HOURS- 000 TO 1000, LST
FROM 1948 3 31 TO 1949 2 23

CLOUD BASE HEIGHT 0.333						
ANG(DEG)	1.0	2.0	3.0	5.0	15.0	45.0 90.0
FREE	768	763	763	765	774	794 806
UNTR	803	804	805	805	804	800 823
SPRO	805	805	805	805	804	800 823
SUPR	768	768	768	768	776	817 782
FALL						
CLOUD BASE HEIGHT 0.666						
ANG(DEG)	1.0	2.0	3.0	5.0	15.0	45.0 90.0
FREE	672	672	674	675	686	709 784
UNTR	858	860	861	862	871	888 883
SPRO	857	858	859	860	869	888 883
SUPR	672	672	671	671	686	711 782
FALL						
CLOUD BASE HEIGHT 1.000						
ANG(DEG)	1.0	2.0	3.0	5.0	15.0	45.0 90.0
FREE	513	514	516	518	530	560 579
UNTR	716	717	719	720	728	757 723
SPRO	716	717	719	720	728	757 723
SUPR	513	514	516	518	530	560 579
FALL						
CLOUD BASE HEIGHT 2.000						
ANG(DEG)	1.0	2.0	3.0	5.0	15.0	45.0 90.0
FREE	488	489	491	494	499	506 490
UNTR	684	685	687	689	694	697 683
SPRO	684	685	687	689	694	697 683
SUPR	488	489	491	494	499	506 490
FALL						

HAMBURG, GERMANY
DAYTIME HOURS- 000 TO 1000, LST
FROM 1949 1 1 TO 1950 2 21

CLOUD BASE HEIGHT 0.333						
ANG(DEG)	1.0	2.0	3.0	5.0	15.0	45.0 90.0
FREE	825	825	827	829	836	853 833
UNTR	798	798	799	800	804	804 824
SPRO	798	798	799	800	804	804 824
SUPR	798	798	799	800	804	804 824
FALL						
CLOUD BASE HEIGHT 0.666						
ANG(DEG)	1.0	2.0	3.0	5.0	15.0	45.0 90.0
FREE	636	637	638	641	655	683 699
UNTR	835	837	838	840	844	849 828
SPRO	835	837	838	840	844	849 828
SUPR	636	637	638	641	655	683 699
FALL						
CLOUD BASE HEIGHT 1.000						
ANG(DEG)	1.0	2.0	3.0	5.0	15.0	45.0 90.0
FREE	393	395	396	399	407	427 427
UNTR	614	615	616	618	624	625 625
SPRO	614	615	616	618	624	625 625
SUPR	393	395	396	399	407	427 427
FALL						
CLOUD BASE HEIGHT 2.000						
ANG(DEG)	1.0	2.0	3.0	5.0	15.0	45.0 90.0
FREE	274	277	278	280	287	293 293
UNTR	498	499	500	501	504	504 504
SPRO	498	499	500	501	504	504 504
SUPR	274	277	278	280	287	293 293
FALL						

NICOSIA, CYPRUS
DAYTIME HOURS- 000 TO 1000, LST
FROM 1949 1 1 TO 1950 11 21

CLOUD BASE HEIGHT 0.333						
ANG(DEG)	1.0	2.0	3.0	5.0	15.0	45.0 90.0
FREE	827	827	829	831	837	853 833
UNTR	827	827	829	831	837	853 833
SPRO	827	827	829	831	837	853 833
SUPR	827	827	829	831	837	853 833
FALL						
CLOUD BASE HEIGHT 0.666						
ANG(DEG)	1.0	2.0	3.0	5.0	15.0	45.0 90.0
FREE	637	638	639	642	656	684 699
UNTR	836	838	839	841	845	850 828
SPRO	836	838	839	841	845	850 828
SUPR	637	638	639	642	656	684 699
FALL						
CLOUD BASE HEIGHT 1.000						
ANG(DEG)	1.0	2.0	3.0	5.0	15.0	45.0 90.0
FREE	394	396	397	400	408	428 428
UNTR	615	616	617	619	625	626 626
SPRO	615	616	617	619	625	626 626
SUPR	394	396	397	400	408	428 428
FALL						
CLOUD BASE HEIGHT 2.000						
ANG(DEG)	1.0	2.0	3.0	5.0	15.0	45.0 90.0
FREE	275	278	279	281	288	294 294
UNTR	499	500	501	502	505	505 505
SPRO	499	500	501	502	505	505 505
SUPR	275	278	279	281	288	294 294
FALL						

ESSEN, GERMANY
DAYTIME HOURS- 000 TO 1000, LST
FROM 1949 1 1 TO 1950 2 4

CLOUD BASE HEIGHT 0.333						
ANG(DEG)	1.0	2.0	3.0	5.0	15.0	45.0 90.0
FREE	648	648	650	652	662	686 701
UNTR	878	879	880	881	885	888 888
SPRO	878	879	880	881	885	888 888
SUPR	648	648	650	652	662	686 701
FALL						
CLOUD BASE HEIGHT 0.666						
ANG(DEG)	1.0	2.0	3.0	5.0	15.0	45.0 90.0
FREE	484	485	486	488	492	525 540
UNTR	784	785	786	787	790	795 795
SPRO	784	785	786	787	790	795 795
SUPR	484	485	486	488	492	525 540
FALL						
CLOUD BASE HEIGHT 1.000						
ANG(DEG)	1.0	2.0	3.0	5.0	15.0	45.0 90.0
FREE	387	389	390	392	396	425 425
UNTR	648	649	650	651	654	655 655
SPRO	648	649	650	651	654	655 655
SUPR	387	389	390	392	396	425 425
FALL						
CLOUD BASE HEIGHT 2.000						
ANG(DEG)	1.0	2.0	3.0	5.0	15.0	45.0 90.0
FREE	178	181	182	183	186	190 190
UNTR	488	489	490	491	493	493 493
SPRO	488	489	490	491	493	493 493
SUPR	178	181	182	183	186	190 190
FALL						

FALMOUTH, MA, USA
DAYTIME HOURS- 000 TO 1000, LST
FROM 1949 1 1 TO 1950 2 21

CLOUD BASE HEIGHT 0.333						
ANG(DEG)	1.0	2.0	3.0	5.0	15.0	45.0 90.0
FREE	793	794	794	795	795	805 820
UNTR	781	782	782	783	784	795 805
SPRO	781	782	782	783	784	795 805
SUPR	793	794	794	795	795	805 820
FALL						
CLOUD BASE HEIGHT 0.666						
ANG(DEG)	1.0	2.0	3.0	5.0	15.0	45.0 90.0
FREE	780	781	781	782	782	794 800
UNTR	780	781	781	782	782	794 800
SPRO	780	781	781	782	782	794 800
SUPR	780	781	781	782	782	794 800
FALL						
CLOUD BASE HEIGHT 1.000						
ANG(DEG)	1.0	2.0	3.0	5.0	15.0	45.0 90.0
FREE	615	616	616	617	618	625 625
UNTR	615	616	616	617	618	625 625
SPRO	615	616	616	617	618	625 625
SUPR	615	616	616	617	618	625 625
FALL						
CLOUD BASE HEIGHT 2.000						
ANG(DEG)	1.0	2.0	3.0	5.0	15.0	45.0 90.0
FREE	400	401	401	402	403	403 403
UNTR	615	616	616	617	618	625 625
SPRO	615	616	616	617	618	625 625
SUPR	400	401	401	402	403	403 403
FALL						

NEW, S. VIETNAM
DAYTIME HOURS- 000 TO 1000, LST
FROM 1949 1 1 TO 1950 2 21

CLOUD BASE HEIGHT 0.333						
ANG(DEG)	1.0	2.0	3.0	5.0	15.0	45.0 90.0
FREE	793	794	794	795	795	805 820
UNTR	781	782	782	783	784	795 805
SPRO	781	782	782	783	784	795 805
SUPR	793	794	794	795	795	805 820
FALL						
CLOUD BASE HEIGHT 0.666						
ANG(DEG)	1.0	2.0	3.0	5.0	15.0	45.0 90.0
FREE	780	781	781	782	782	794 800
UNTR	780	781	781	782	782	794 800
SPRO	780	781	781	782	782	794 800
SUPR	780	781	781	782	782	794 800
FALL						
CLOUD BASE HEIGHT 1.000						
ANG(DEG)	1.0	2.0	3.0	5.0	15.0	45.0 90.0
FREE	615	616	616	617	618	625 625
UNTR	615	616	616	617	618	625 625
SPRO	615	616	616	617	618	625 625
SUPR	615	616	616	617	618	625 625
FALL						
CLOUD BASE HEIGHT 2.000						
ANG(DEG)	1.0	2.0	3.0	5.0	15.0	45.0 90.0
FREE	400	401	401	402	403	403 403
UNTR	615	616	616	617	618	625 625
SPRO	615	616	616	617	618	625 625
SUPR	400	401	401	402	403	403 403
FALL						

REFERENCES

1. E. Rodriguez and R. Huschke, "The RAND Weather Data Bank (RAWDAB): An Evolving Base of Accessible Weather Data," RAND Report R-1269-PR (March 1974).
2. J. Selby and R. McClatchey, "Atmospheric Transmittance from 0.25 to 28.6 μ m: Computer Code LOWTRAN 2," Air Force Cambridge Research Laboratories Report AFCRL-72-0745 (29 December 1972).
3. "AWS Data Families 12-13: Electronic Data Processing Reference Manual (Synoptic Observation, Chapter 3, The Observations)," Vols. I and II (September 1960).
4. L. Biberman and G. duMais, "Modeling the Effects of Weather on 8.5-11 Micrometer FLIR Performance: An Analysis Using Real Data," IDA Technical Report (1975).
5. H. Barhydt, "Sea Level Atmospheric Transmission in the 8-11.5 μ Band," Interdepartmental Correspondence, Hughes Aircraft Company (May 1974).
6. J. McCoy, D. Rensch and F. Long, "Water Vapor Continuum Absorption of Carbon Dioxide Laser Radiation Near 10 μ ," Appl. Opt. 7, 1471 (1969).
7. R. McClatchey and J. Selby, "Atmospheric Attenuation of Laser Radiation from 0.76 to 31.25 μ m," Air Force Cambridge Research Laboratories Report AFCRL-TR-74-0003 (3 January 1974).
8. R. G. Eldridge, Bull. Am. Meteorol. Soc. 50, 422 (1969).
9. E. O. Hulbert, J. Opt. Soc. Am. 31, 467 (1941).
10. D. B. Rensch and R. K. Long, "Comparative Studies of Extinction and Backscattering by Aerosols, Fog, and Rain at 10.6 μ and 0.63 μ ," Appl. Opt. 9 1563 (1970).
11. J. Rosen and C. Schutz, "The Effectiveness of a New Air Defense Weapon in Cloudy Weather: Methodology and Applications," RAND Report R-1256-ARPA (December 1973).
12. Y. Lubkin, An Introduction to Correlation, (Federal Scientific Corporation, New York, 1 May 1973).

18-5-6371

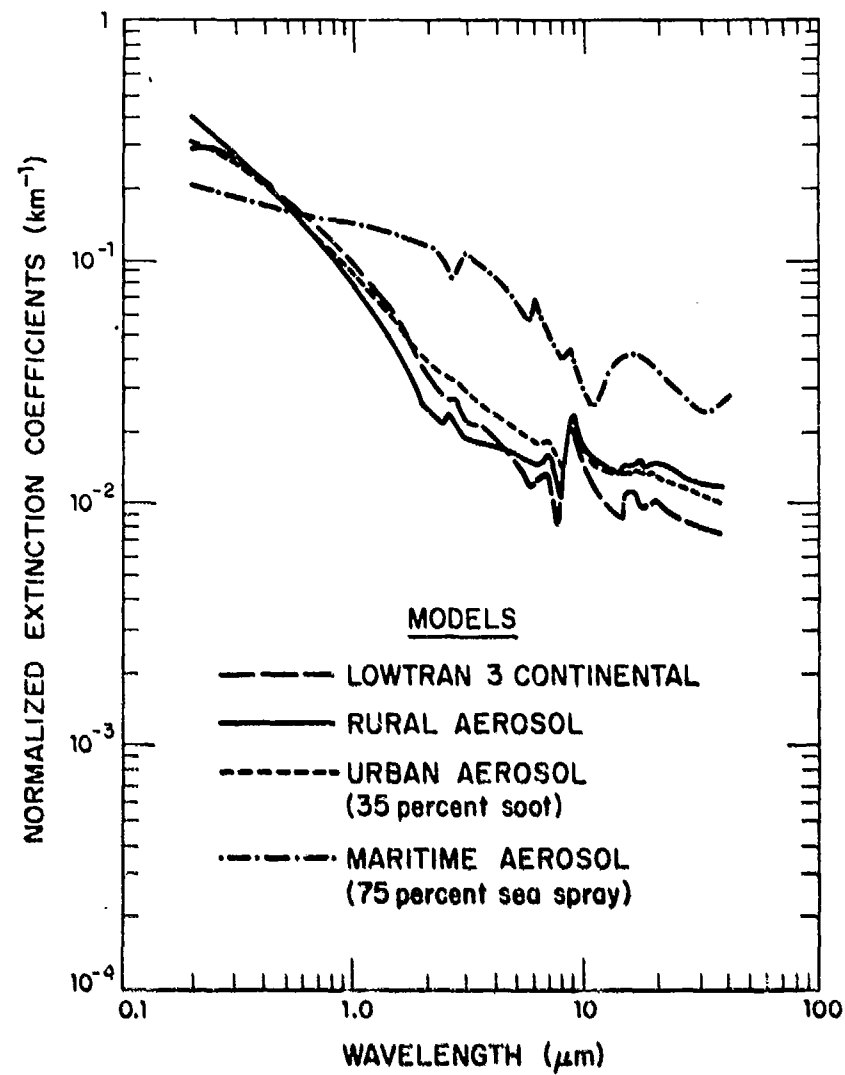
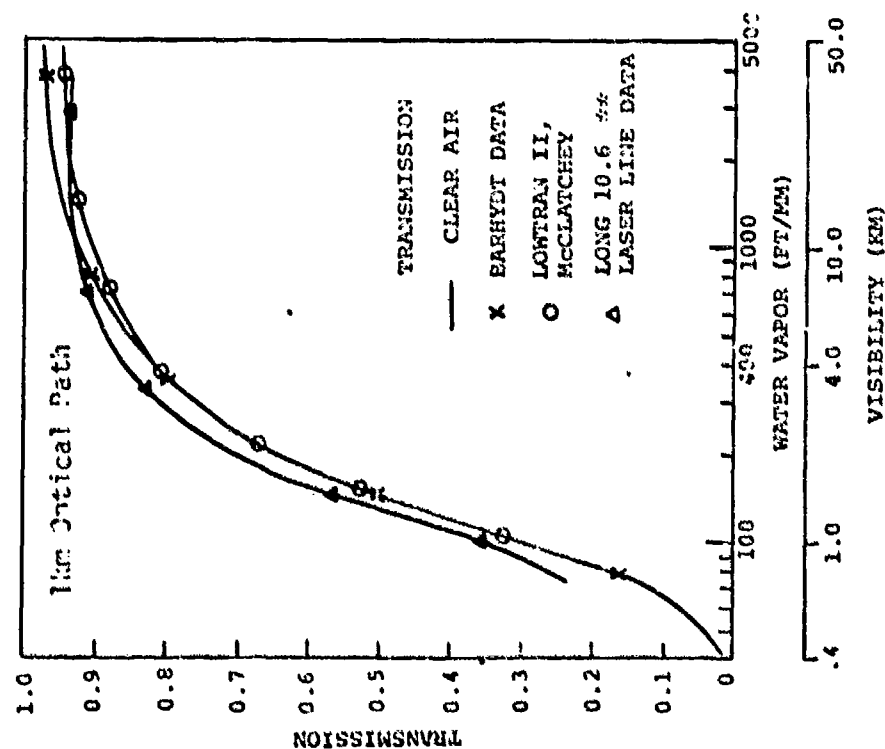


Fig. 1. Aerosol normalized extinction coefficients.

INFRARED ATMOSPHERIC TRANSMISSION
MODELS IN THE 8 - 11.5 μ m BAND



II-7 (2)

INFRARED ATMOSPHERIC TRANSMISSION
MODELS IN THE 8 - 11.5 μ m BAND

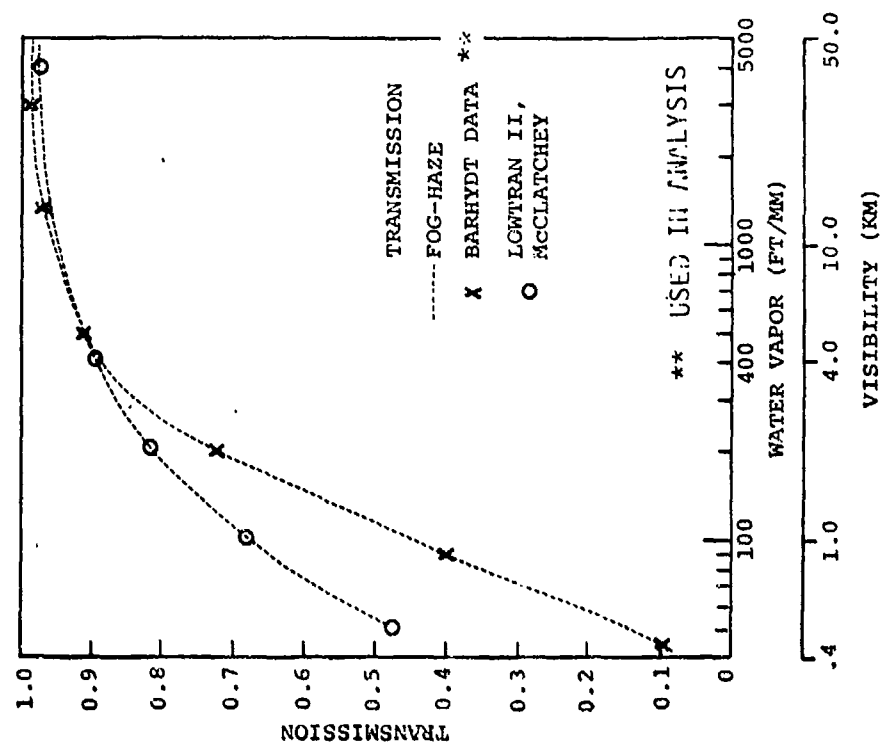


Fig. 2. Comparison of atmospheric attenuation models for clear-air and fog-haze transmission in the 8-11.5 μ m IR band.

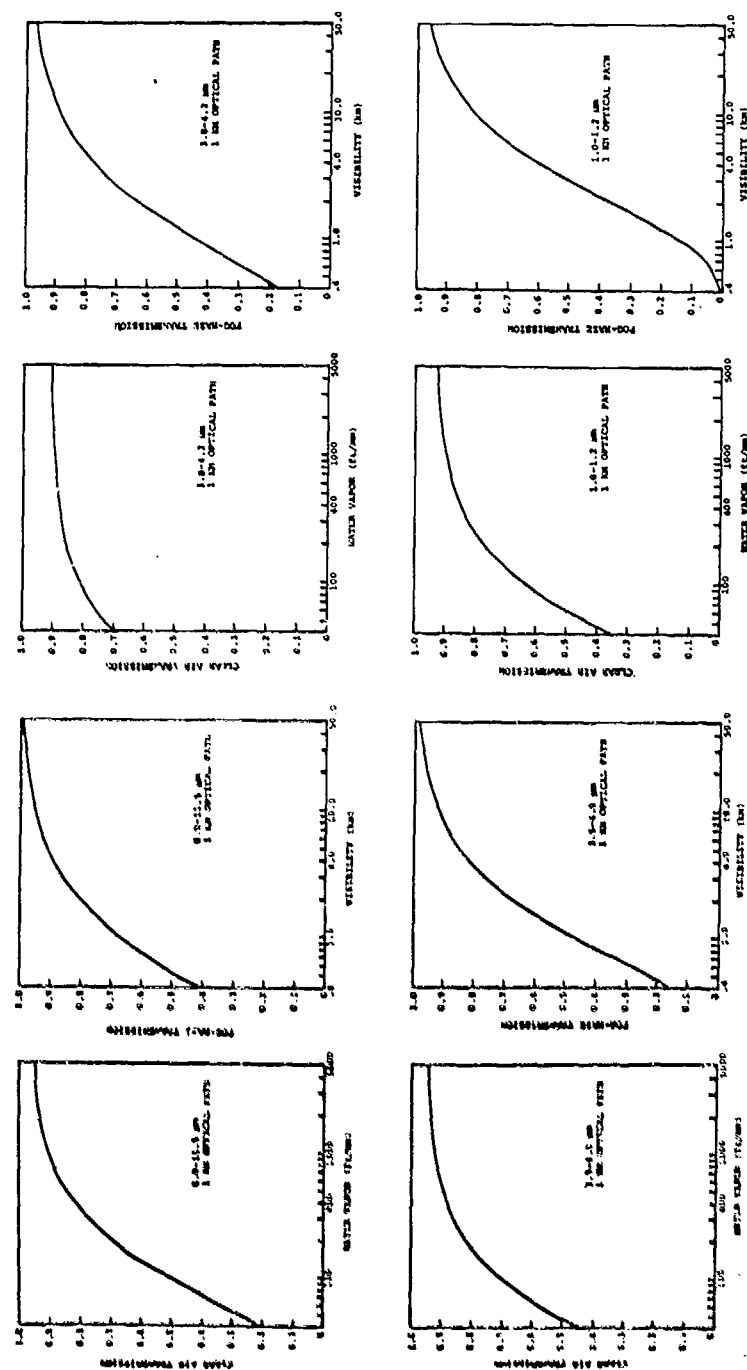


Fig. 3. LOWTRAN clear-air and rural fog-haze transmission curves for several atmospheric windows in the 1.0-14.0μm IR spectral band.

18-5-6702

SLANT RANGE SCALE FACTOR

$$\Delta = L^{-1} \operatorname{cosec} \phi \int_0^L \exp \left(-\frac{h}{H_0} \right) dh$$

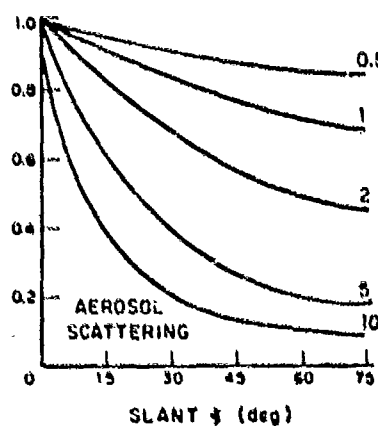
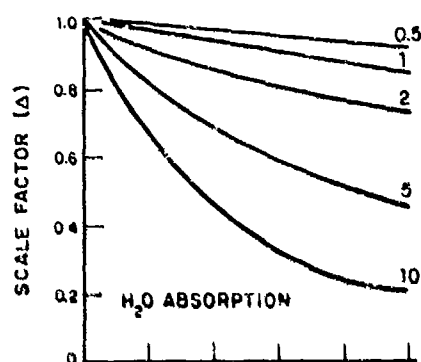
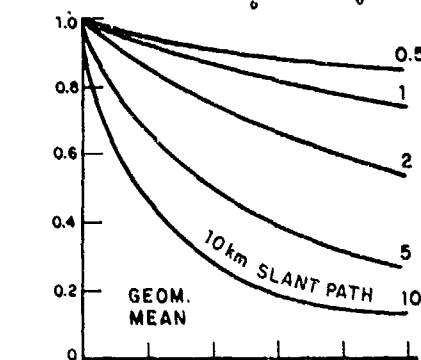


Fig. 4. Slant path correction factors for horizontal atmospheric attenuation losses.

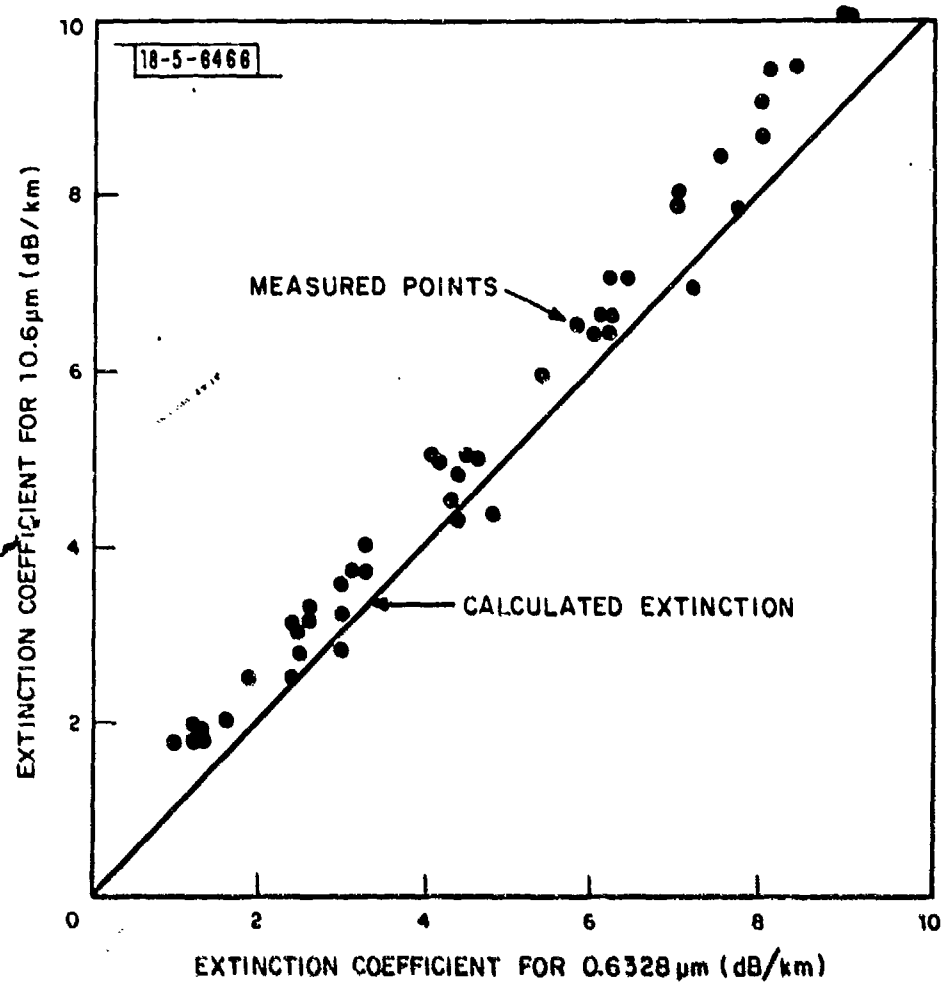
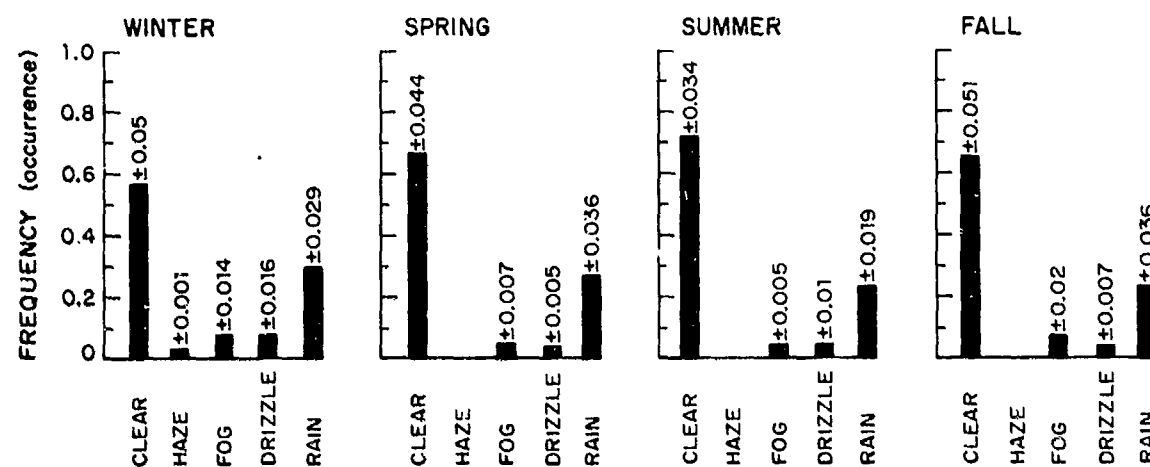
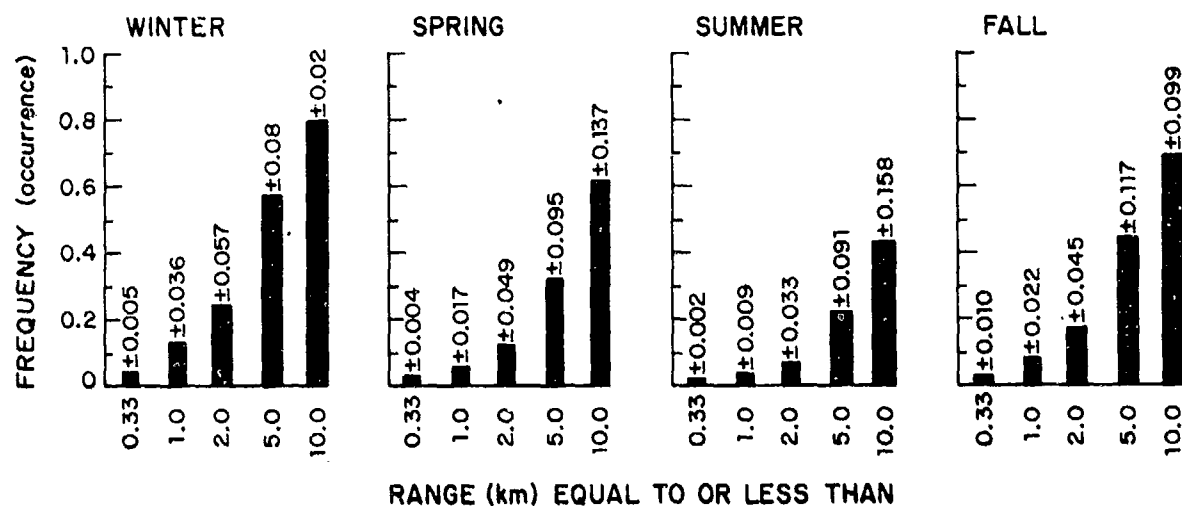


Fig. 5. Experimental and theoretical IR extinction coefficients through rain.



SYNOPTIC WEATHER - AVERAGE: GERMANY
(Dresden, Hamburg, Essen)

Fig. 6. Synoptic weather averages for Germany.



VISIBILITY WEATHER-AVERAGE: GERMANY
(Berlin, Dresden, Essen, Hamburg)

Fig. 7. Average meteorological visibilities for Germany.

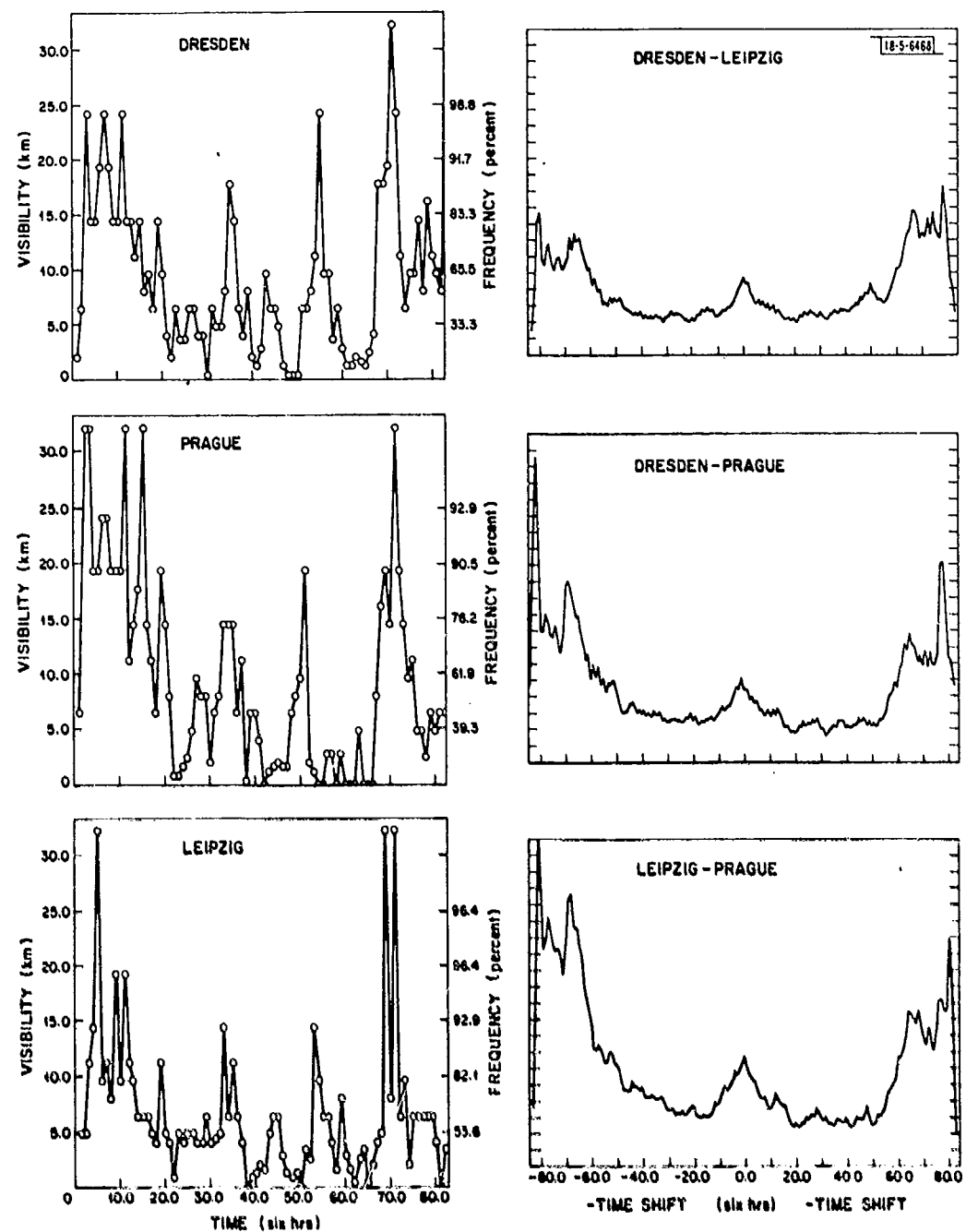
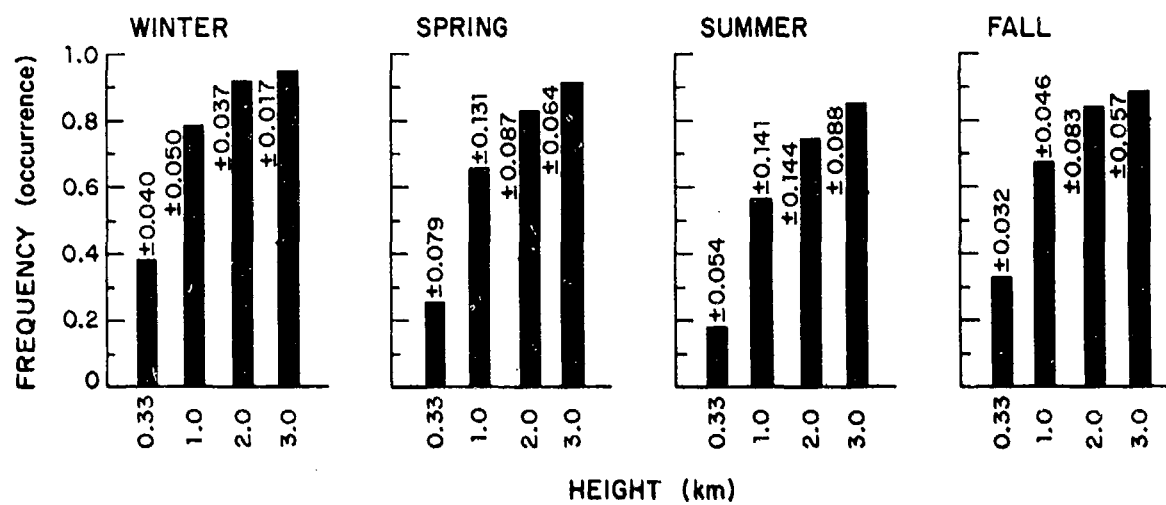


Fig. 8. Short-term visibility and cross-correlation for three European cities.



CLOUD CEILING AVERAGE: GERMANY
(Berlin, Essen, Hamburg)

Fig. 9. Cloud ceiling height averages for Germany.

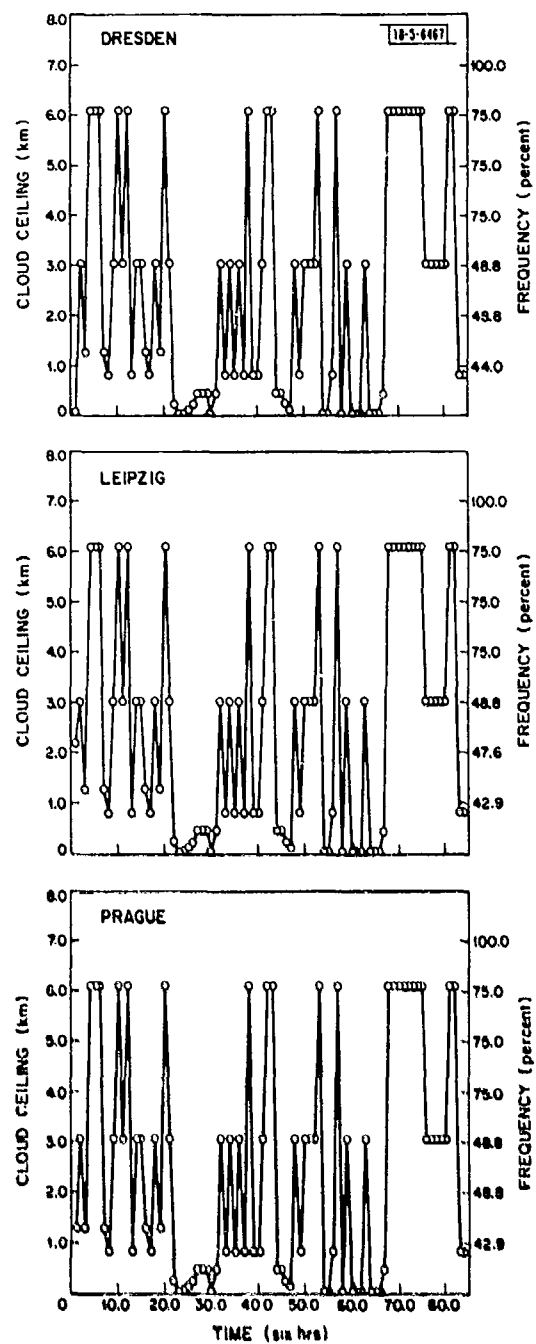


Fig. 10. Short-term variability of cloud ceiling height for three European cities.

IR ATTENUATION LOSS; AVERAGE, GERMANY
DAYTIME HOURS 0600 TO 1800 LST

18-5-6469

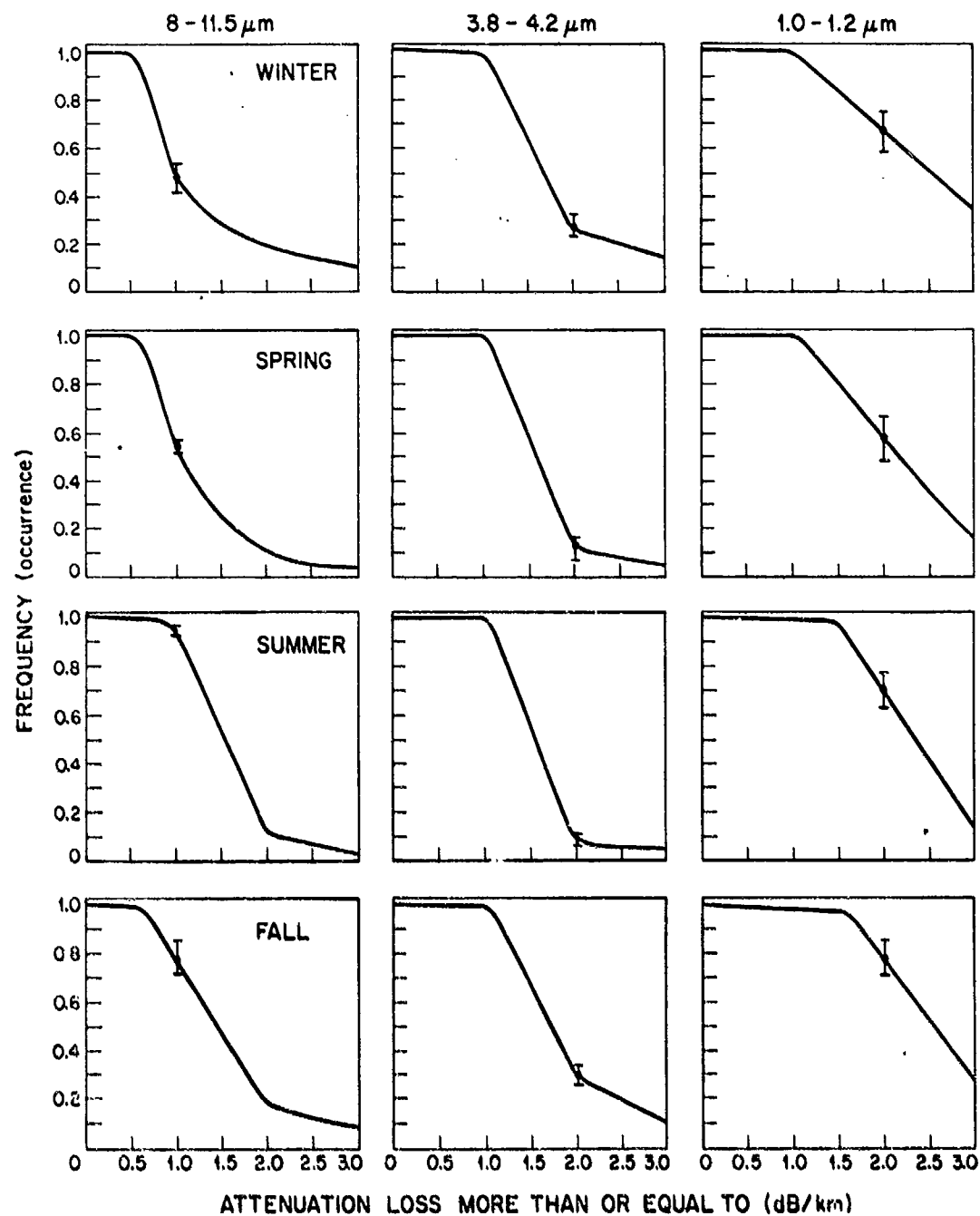


Fig. 11. German average IR attenuation losses for the (1.0-1.2), (3.8-4.2), and (8.0-11.5) μm wavelength bands.

RAIN ATTENUATION LOSS; AVERAGE, GERMANY
DAYTIME HOURS 0600 TO 1800 LST

18-5-6470

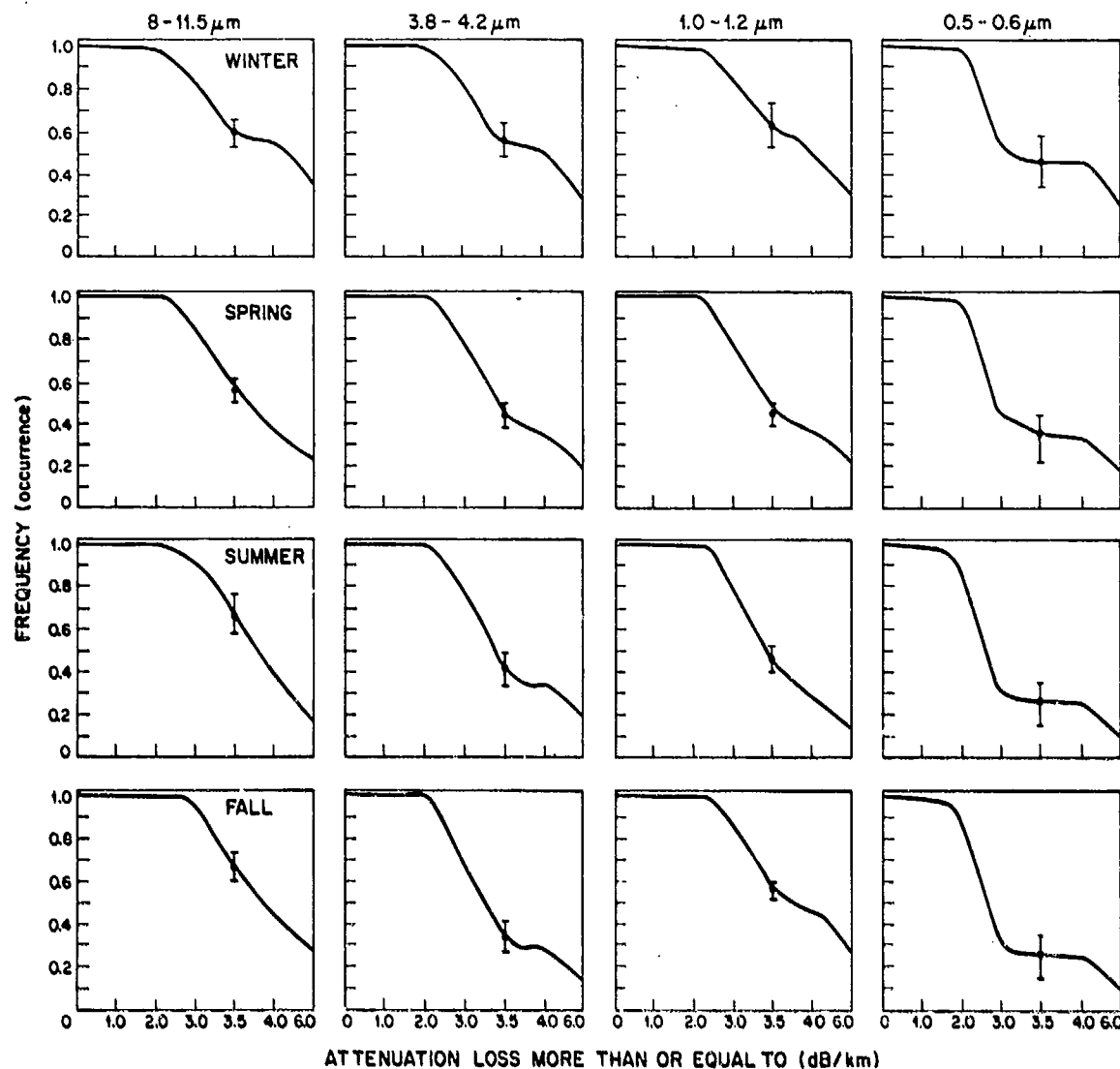


Fig. 12. Average rain attenuation losses in Germany.

18-5-6367

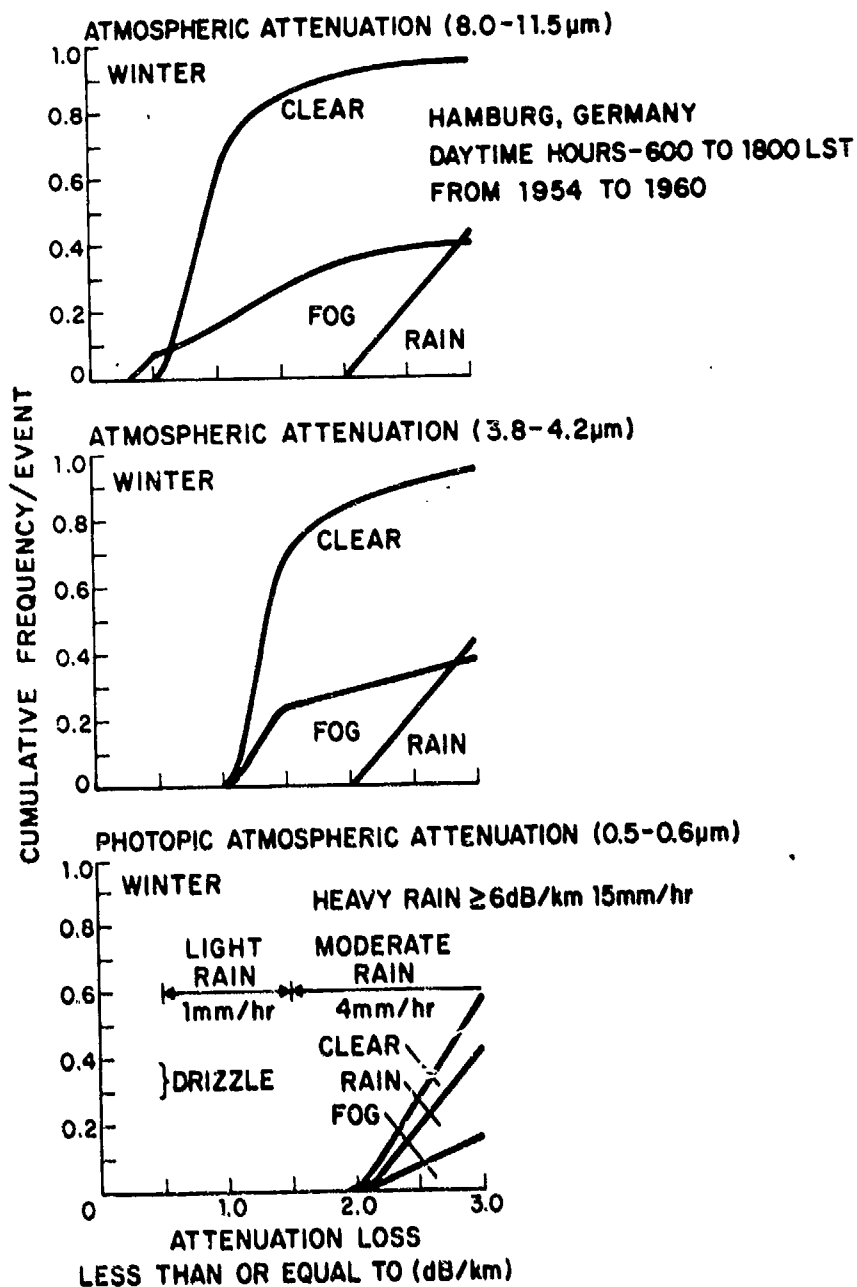


Fig. 13. Comparison of atmospheric attenuation losses for clear weather, fog-haze and rain during winter for Hamburg, Germany.

Meteorological data not available.

Fig. A 1.1 Probability of Synoptic Weather

TT-7 (A 1.2)

BERLIN, GERMANY
DAYTIME HOURS-600 TO 1800 LST
FROM 1946 3 31 TO 1947 5 23

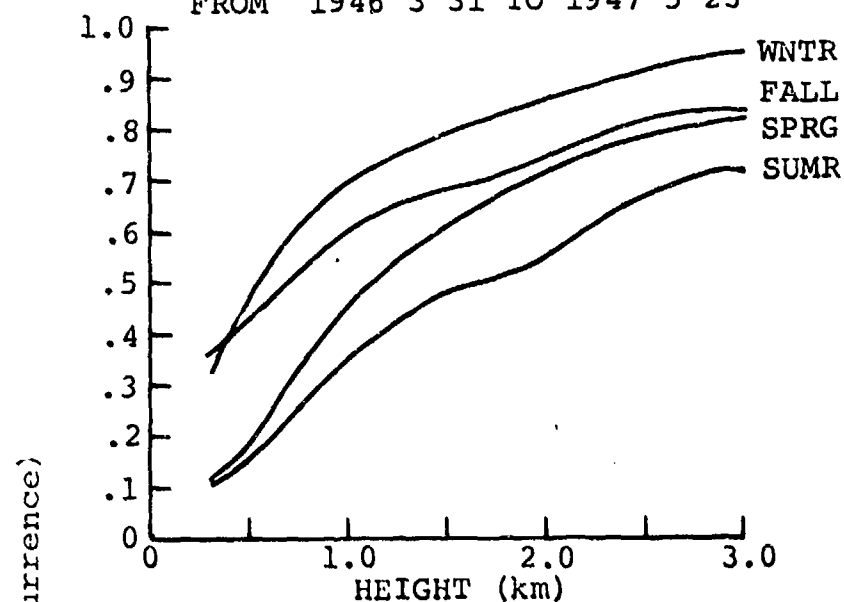


Fig. A 1.2 Probability of Cloud Ceiling Height

TT-7 (A1.3)

BERLIN, GERMANY
DAYTIME HOURS-600 TO 1800 LST
FROM 1946 3 31 TO 1947 5 23

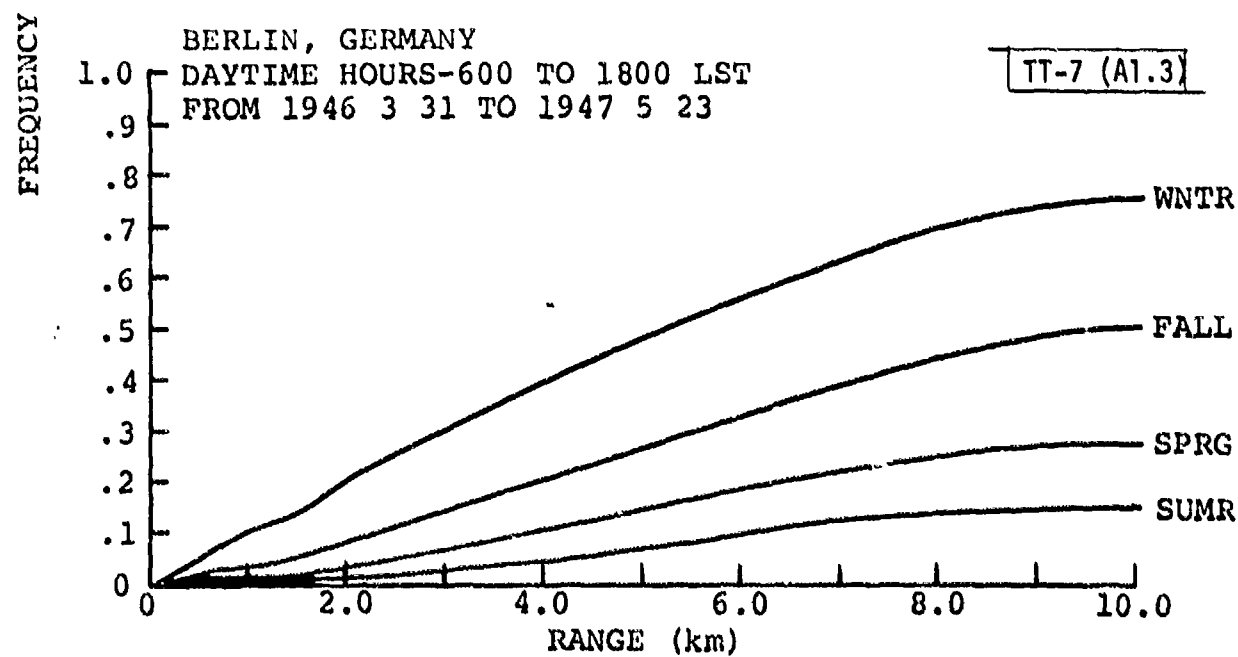


Fig. A 1.3 Probability of Photopic Visibilities

TT-7 (A1.4)

BERLIN, GERMANY
DAYTIME HOURS-600 TO 1800 LST
FROM 1946 3 31 TO 1947 5 23

ATMOSPHERIC ATTENUATION

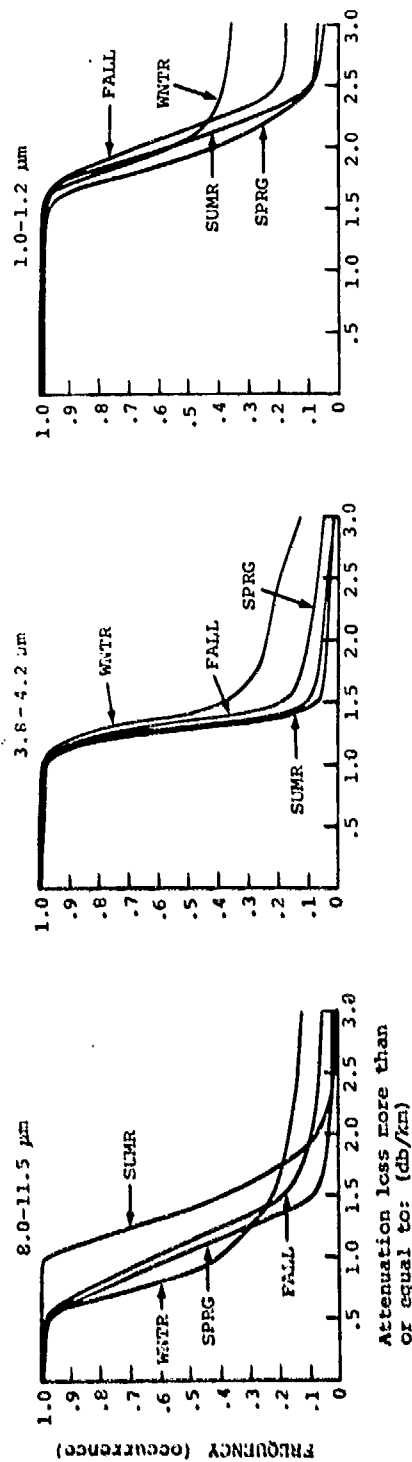


Fig. A 1.4 Probability of Clear Air/Fog-Haze Atmospheric Attenuation for IR Radiation Bands

TT-7 (A1,5)

REF: 14 CLOUDY
DATA: 1465-1955 TO 1955 LST
FROM 1966 1 1: TO 1967 5 23

ATMOSPHERIC ATTENUATION

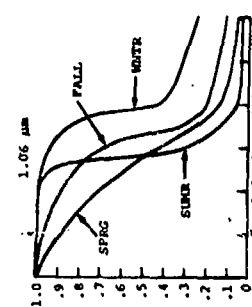
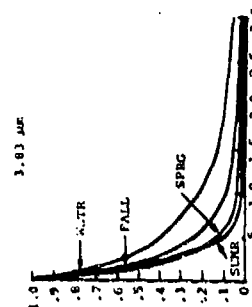
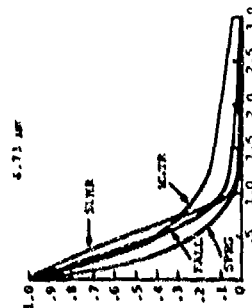
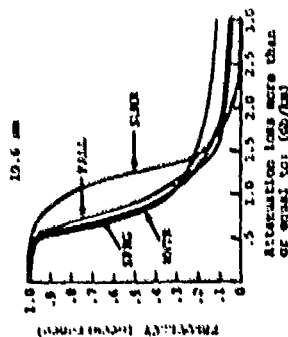


Fig. A 1.5 Probability of Clear Air/Fog-Haze Atmospheric Attenuation for Laser Lines

BERLIN, GERMANY
 DAYTIME HOURS - 600 TO 1800 LST
 FROM 1946 3 31 TO 1947 5 23
 8.0 - 11.5 μm

-5-6711

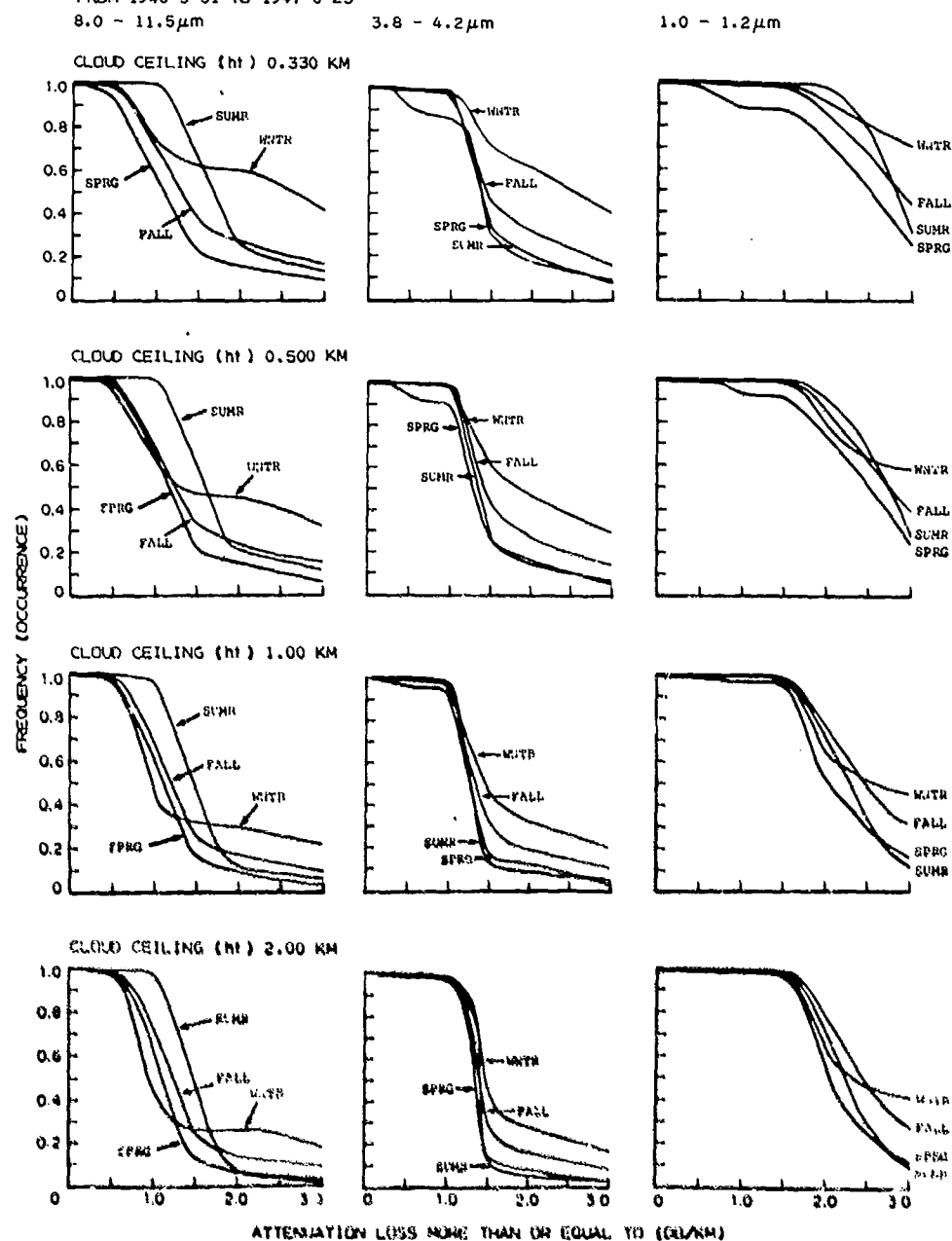


Fig. A 1.6 Joint Probability of Cloud Height and Clear Air/Fog-Haze Attenuation for IR Radiation Bands

BERLIN, GERMANY
DAYTIME HOURS - 600 TO 1800 LST
FROM 1946 3 31 TO 1947 5 23

-5-6706

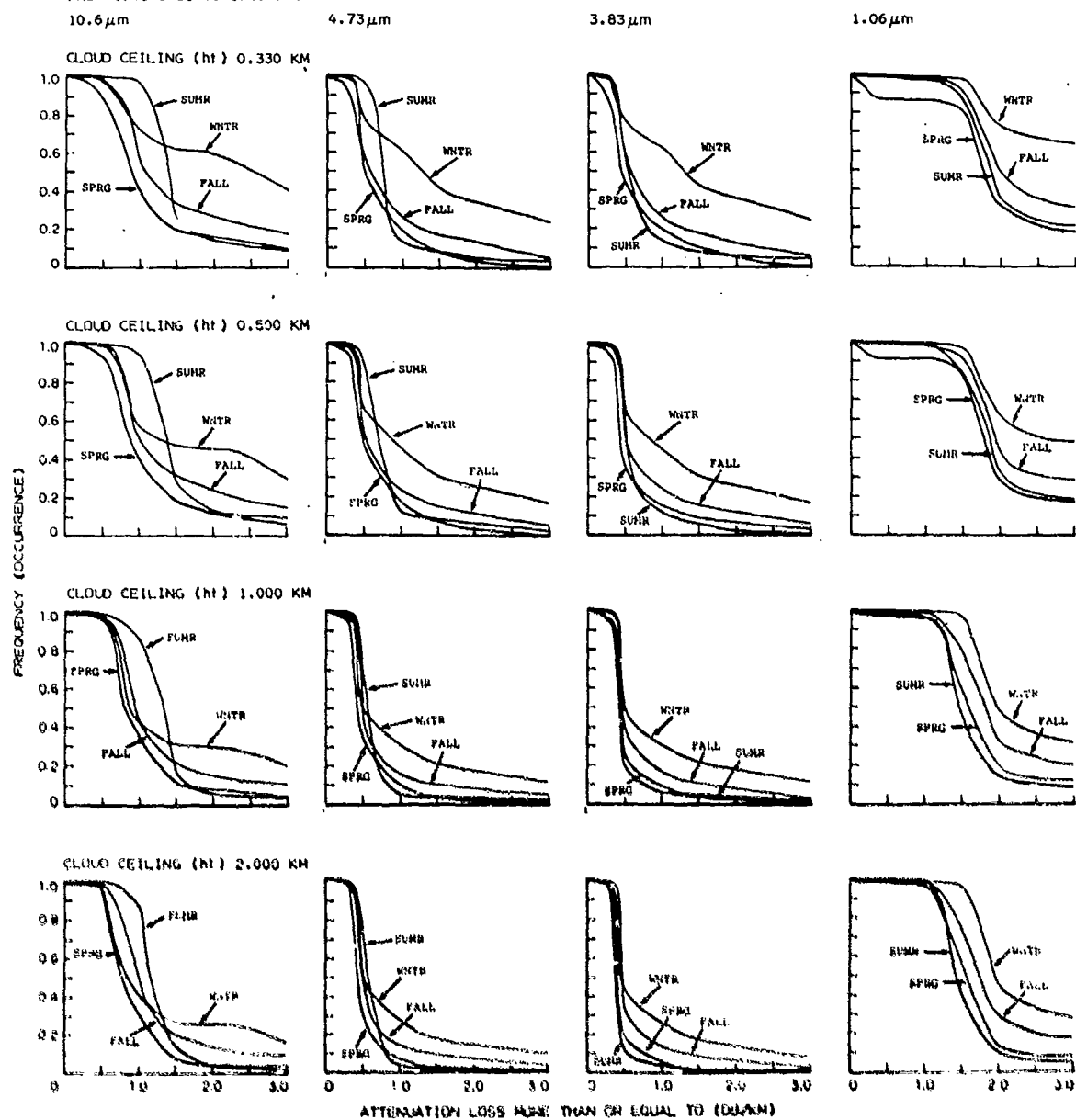


Fig. A 1.7 Joint Probability of Cloud Height and Clear Air/Fog-Haze Attenuation for Laser Lines

TT-7 (A2.1)

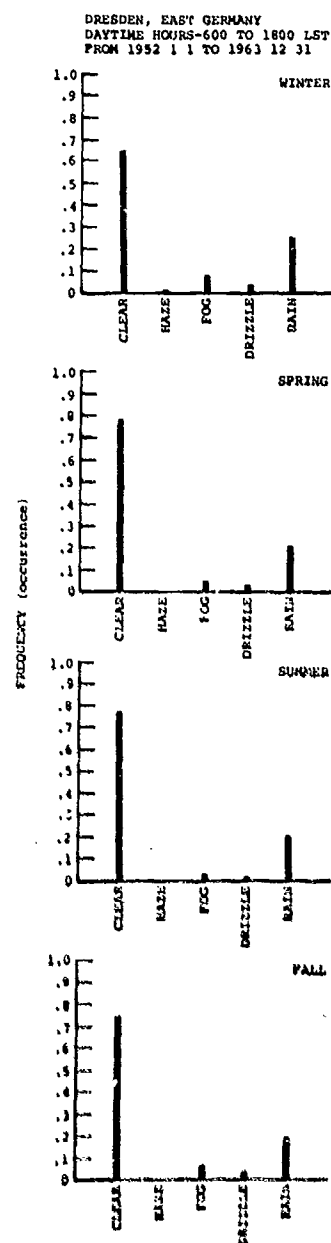


Fig. A 2.1 Probability of Synoptic Weather

Meteorological data not available.

Fig. A 2.2 Probability of Cloud Ceiling Height

TT-7 (A2.3)

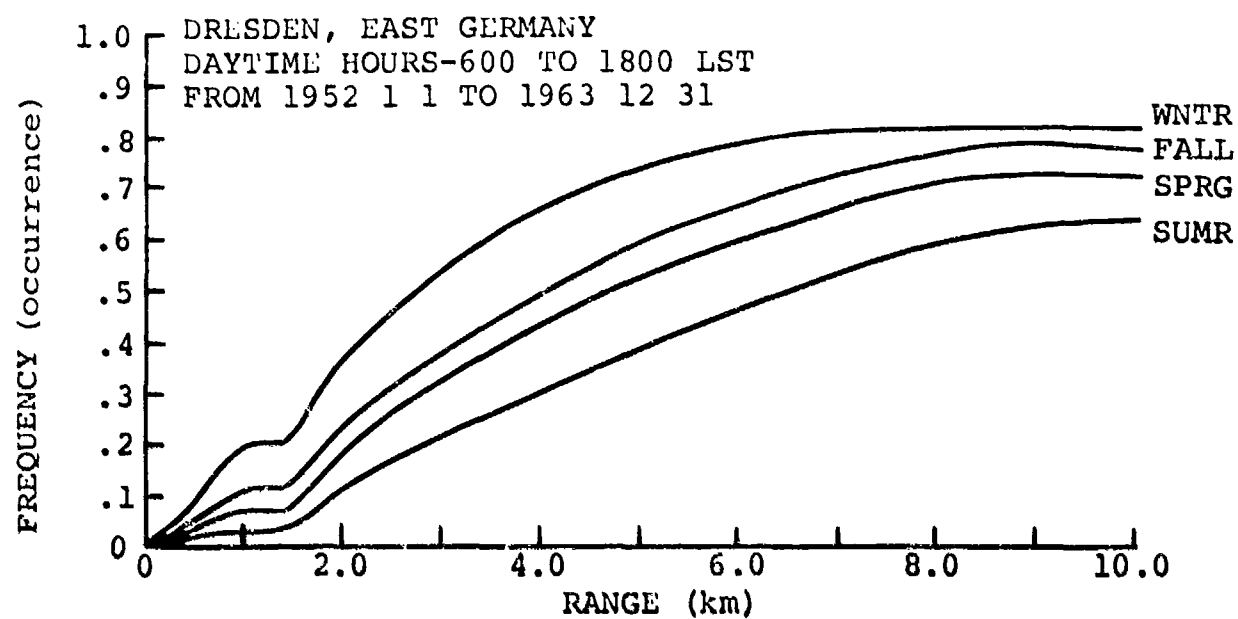


Fig. A 2.3 Probability of Photopic Visibilities

TT-7 (A2.4)

DRESDEN, EAST GERMANY
DAYTIME HOURS-600 TO 1800 LST
FROM 1952 1 1 TO 1958 11 5

ATMOSPHERIC ATTENUATION:

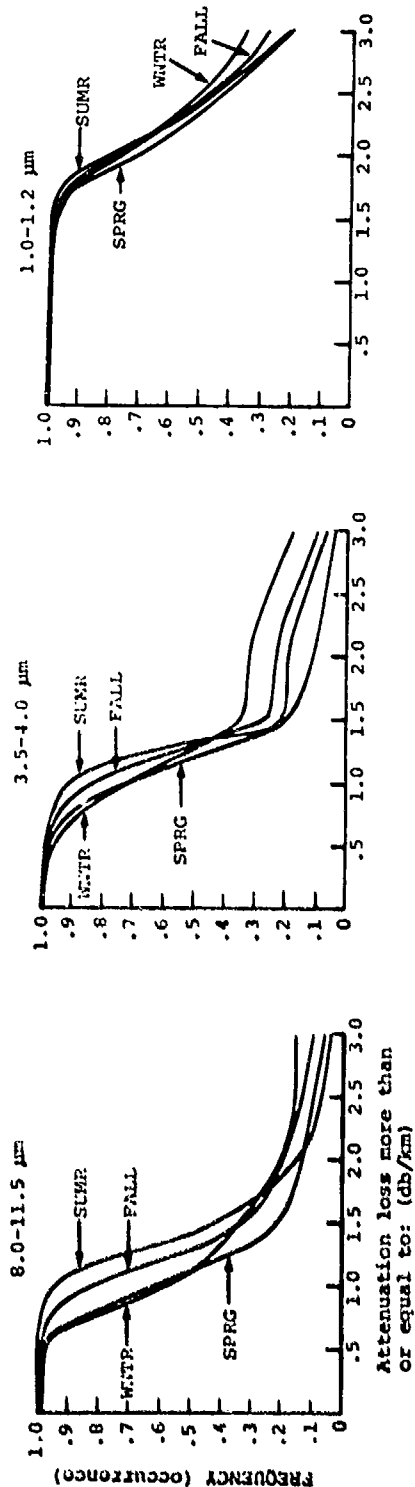
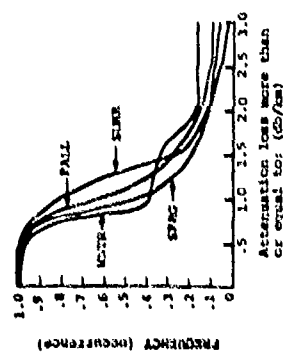


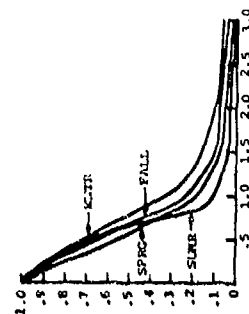
Fig. A 2.4 Probability of Clear Air/Fog-Haze Atmospheric Attenuation for IR Radiation Bands

DRESDEN, EAST GERMANY
 DAYTIME HOURS-600 TO 1800 LT
 FROM 1952 1 1 TO 1958 11 5

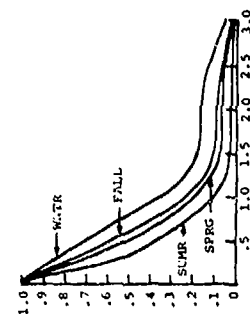
ATMOSPHERIC ATTENUATION
 10.6 μ m



4.73 μ m



3.83 μ m



1.06 μ m

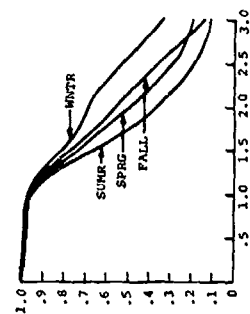


Fig. A 2.5 Probability of Clear Air/Fog-Haze Atmospheric Attenuation
 for Laser Lines

TT-7 (A2,5)

Joint meteorological data not available.

Fig. A 2.6 Joint Probability of Cloud Height and Clear Air/Fog-Haze
Attenuation for IR Radiation Bands

Joint meteorological data not available.

Fig. A 2.7 Joint Probability of Cloud Height and Clear Air/Fog-Haze
Attenuation for Laser Lines

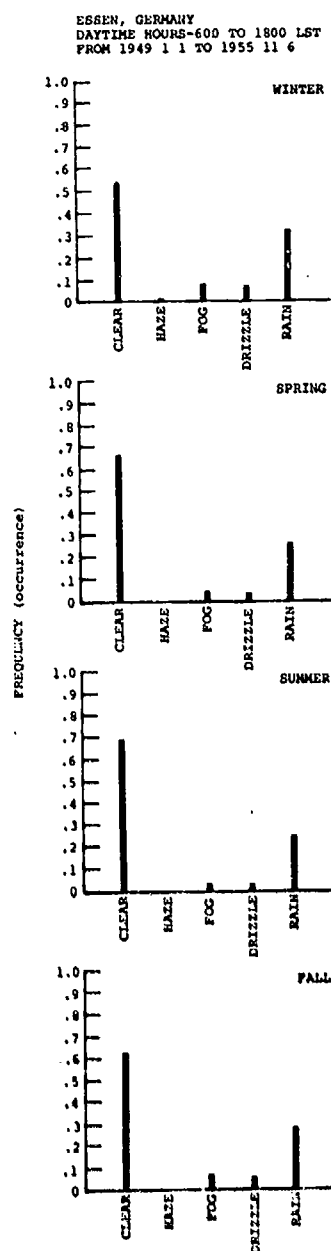


Fig. A 3.1 Probability of Synoptic Weather

TT-7 (A3.2)

ESSEN, GERMANY
DAYTIME HOURS-600 TO 1800 LST
FROM 1949 1 1 TO 1952 6 4

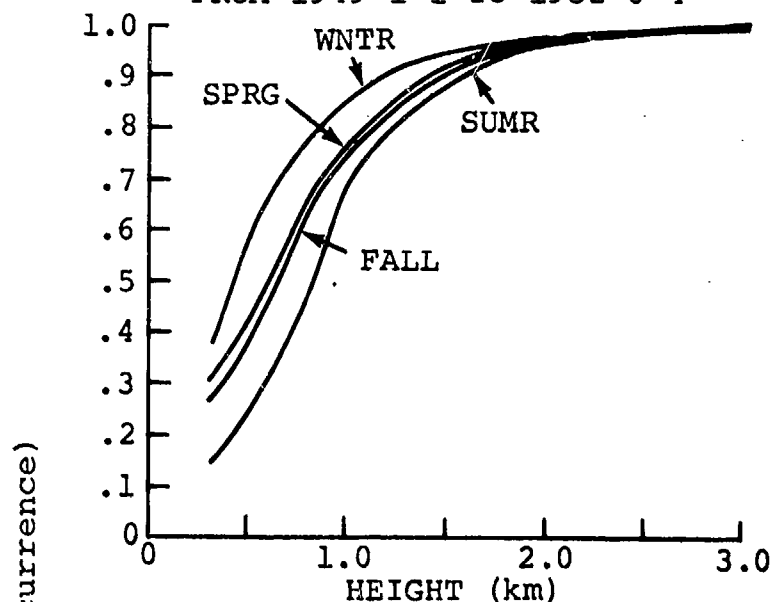


Fig. A 3.2 Probability of Cloud Ceiling Height

TT-7 (A3.3)

ESSEN, GERMANY
DAYTIME HOURS-600 TO 1800 LST
FROM 1949 1 1 TO 1952 6 3

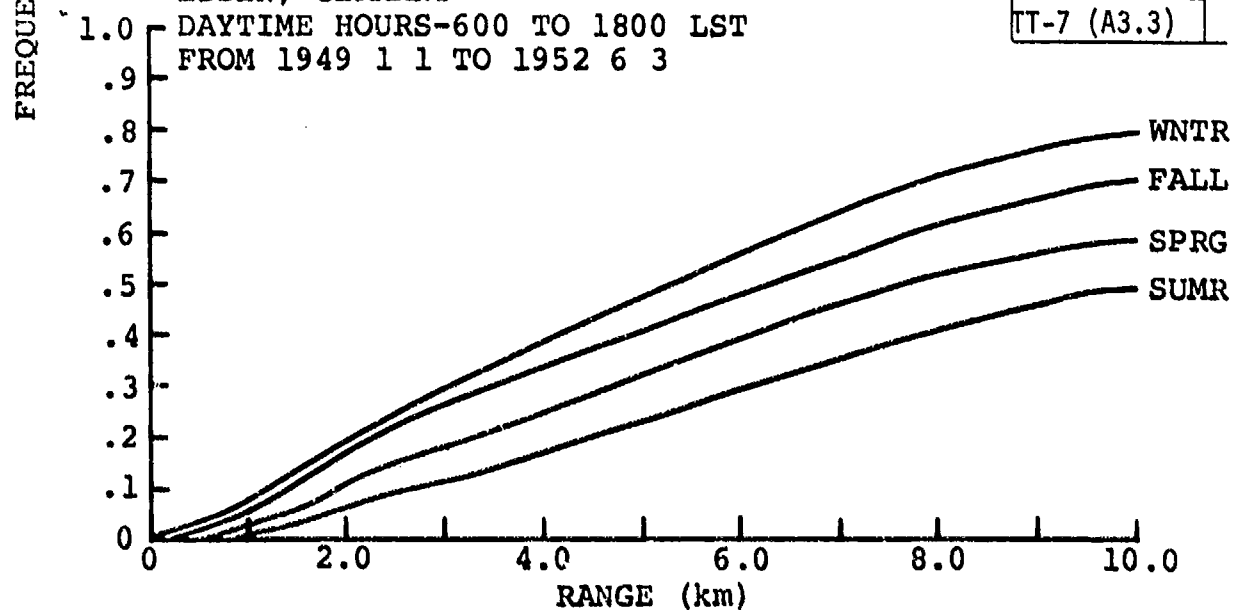


Fig. A 3.3 Probability of Photopic Visibilities

TT-7 (A3.4)

ESSEN, GERMANY
DAYTIME HOURS-600 TO 1800 LST
FROM 1949 1 1 TO 1952 6 2

ATMOSPHERIC ATTENUATION

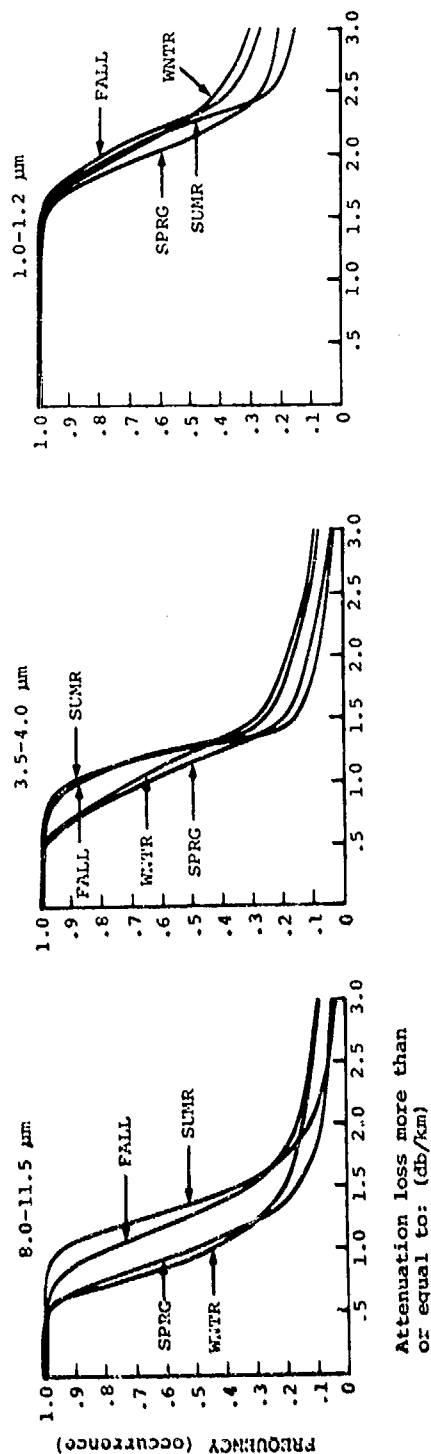


Fig. A 3.4 Probability of Clear Air/Fog-Haze Atmospheric Attenuation for IR Radiation Bands

ESSEN, GERMANY
DAYTIME HOURS-600 TO 1800 LS;
FEB 1949 1 1 TO 1952 6 2

ATMOSPHERIC ATTENUATION:

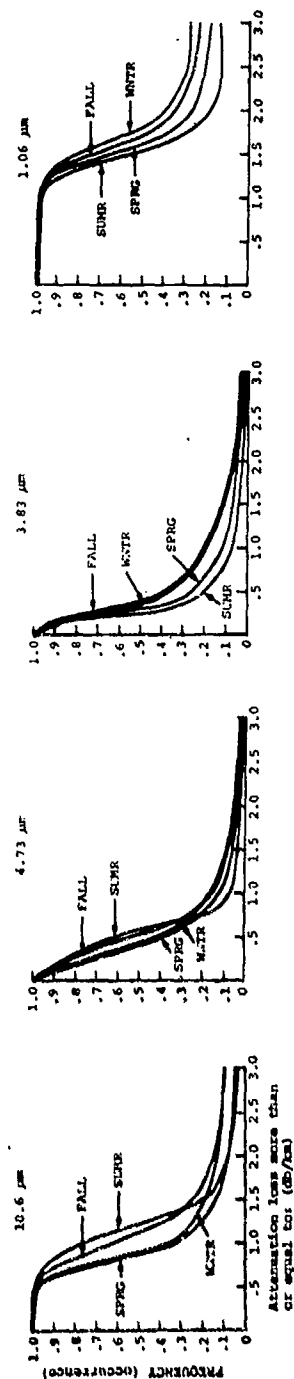


Fig. A 3.5 Probability of Clear Air/Fog-Haze Atmospheric Attenuation for Laser Lines

TT-7 (A3.5)

ESSEN, GERMANY
 DAYTIME HOURS - 600 TO 1800 LST
 FROM 1949 1 1 TO 1952 5 31
 8.0 - 11.5 μm

-5-6705

3.8 - 4.2 μm

1.0 - 1.2 μm

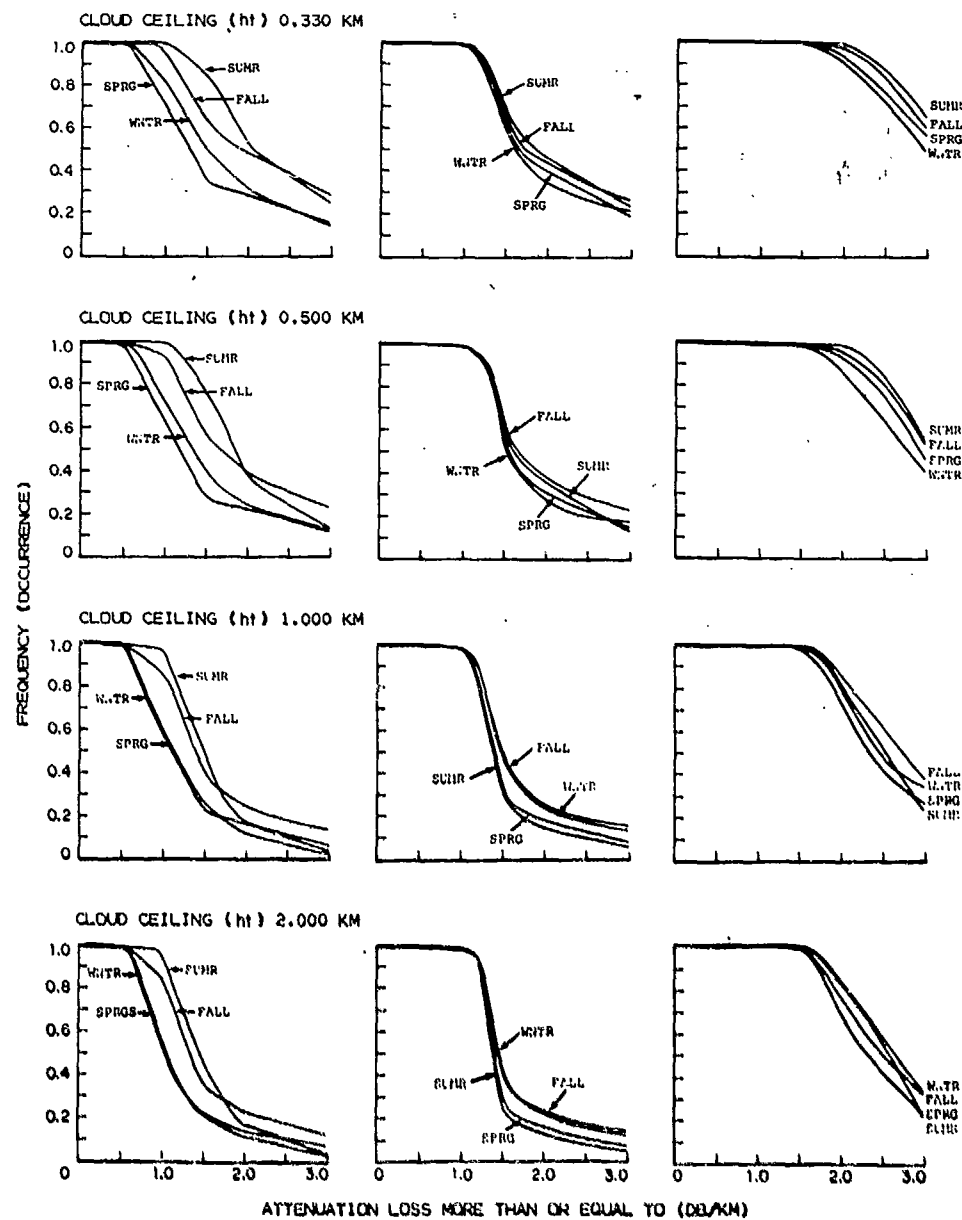


Fig. A 3.6 Joint Probability of Cloud Height and Clear Air/Fog-Haze Attenuation for IR Radiation Bands

ESSEN, GERMANY
DAYTIME HOURS - 600 TO 1800 LST
FROM 1949 1 1 TO 1952 6 1

-5-6712

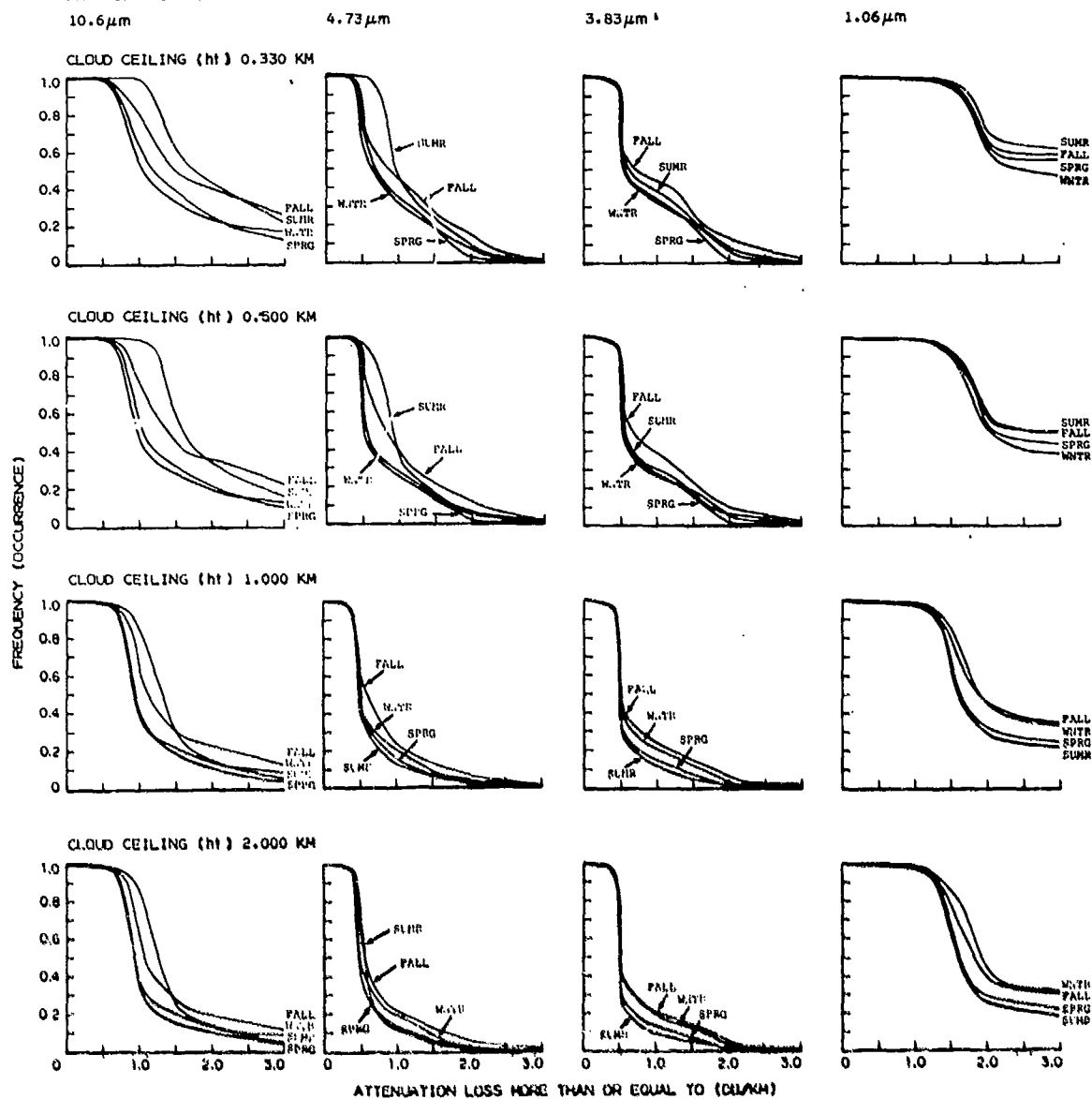


Fig. A 3.7 Joint Probability of Cloud Height and Clear Air/Fog-Haze Attenuation for Laser Lines

TT-7 (A4.1)

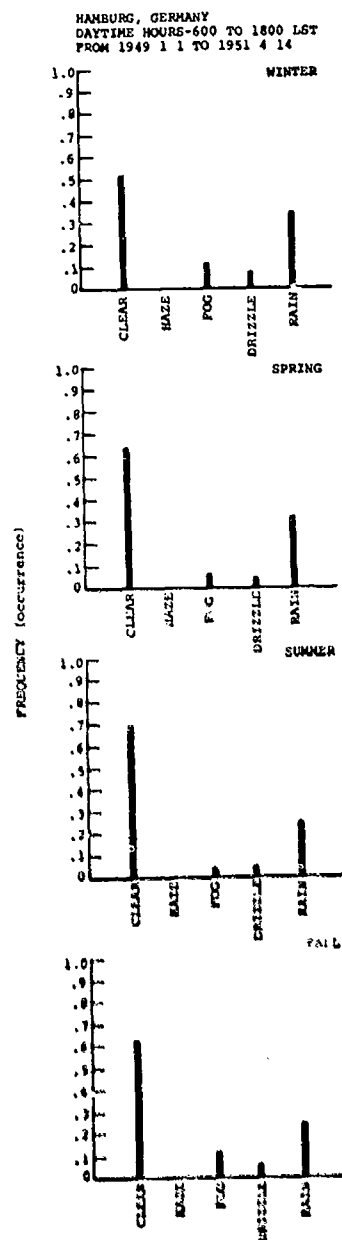


Fig. A 4.1 Probability of Synoptic Weather

HAMBURG, GERMANY
DAYTIME HOURS-600 TO 1800 LST
FROM 1949 1 1 TO 1950 2 21

TT-7 (A4.2)

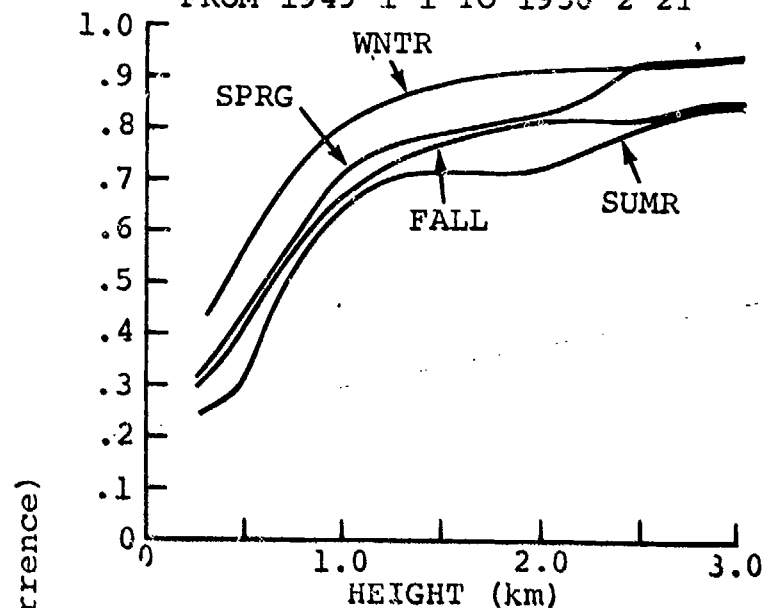


Fig. A 4.2 Probability of Cloud Ceiling Height

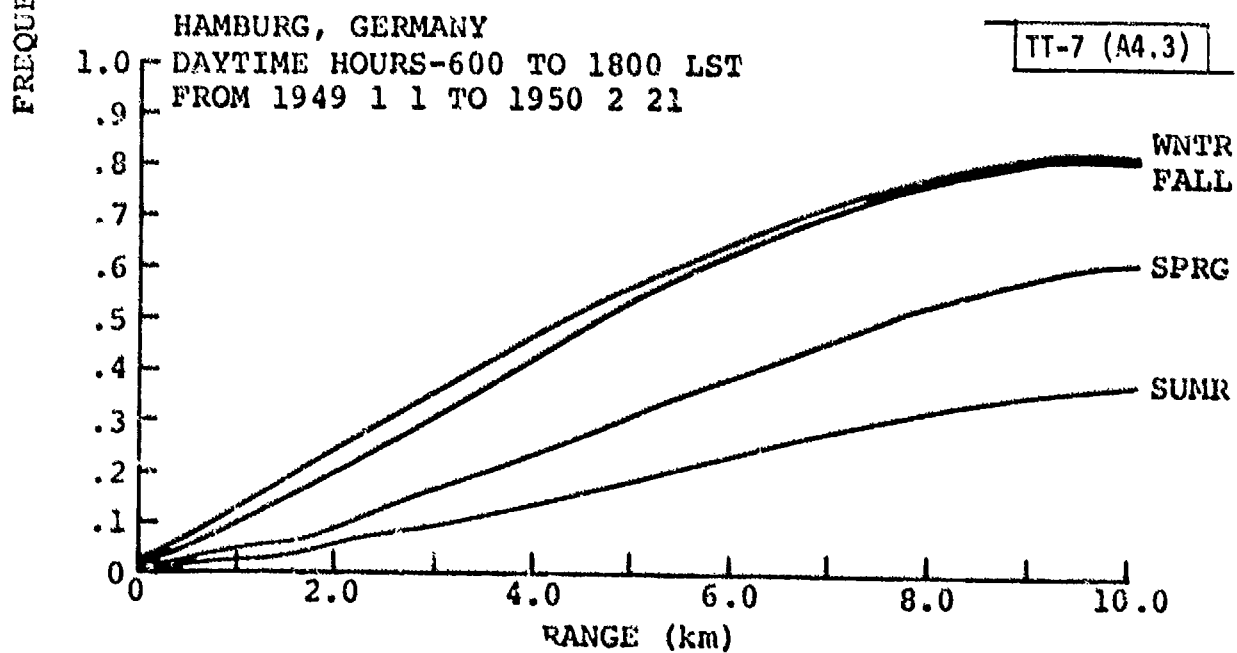
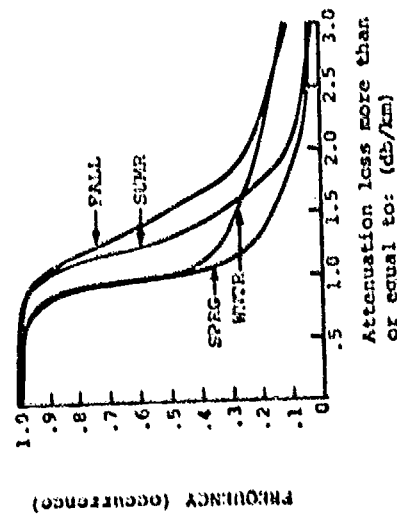


Fig. A 4.3 Probability of Photopic Visibilities

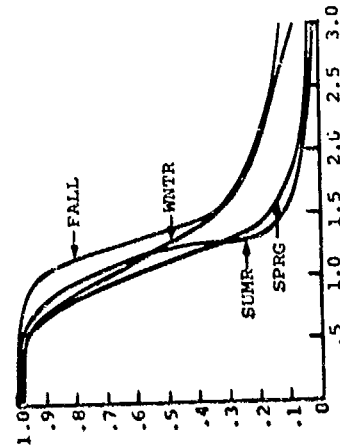
HAMBURG, GERMANY
DAYTIME HOURS-600 TO 1800 LST
FROM 1949 1 1 TO 1950 2 21

TT-7 (A4.4)

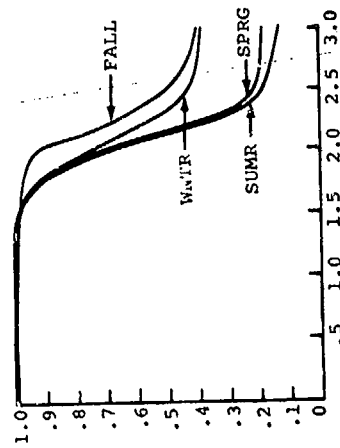
ATMOSPHERIC ATTENUATION
8.0-11.5 μm



3.5-4.0 μm



1.0-1.2 μm

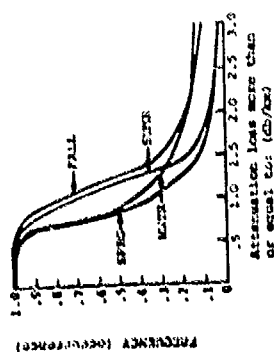


7-75-53-108

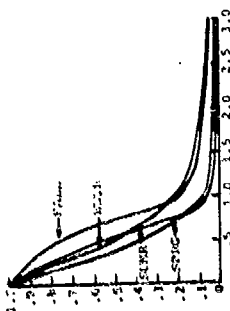
Fig. A 4.4 Probability of Clear Air/Fog-Haze Atmospheric Attenuation
for IR Radiation Bands

BASELINE CORRECTION
DAYTIME, 1948-50 TO 1950-51
FROM 1948 1.1 TO 1950 2.31

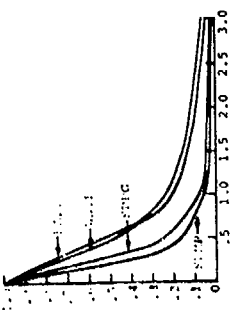
ATMOSPHERIC ATTENUATION
19.6 km



19.6 km



1.83 km



1.06 km

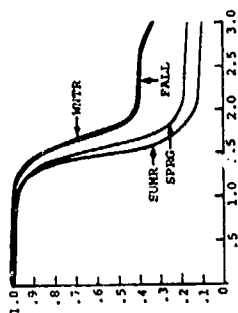


Fig. A 4.5 Probability of Clear Air/Fog-Haze Atmospheric Attenuation
for Laser Lines

TT-7 (A4.5)

HAMBURG, GERMANY
DAYTIME HOURS - 600 TO 1800 LST
FROM 1949 1 1 TO 1950 2 21

-5-8709

8.0 - 11.5 μm

3.8 - 4.2 μm

1.0 - 1.2 μm

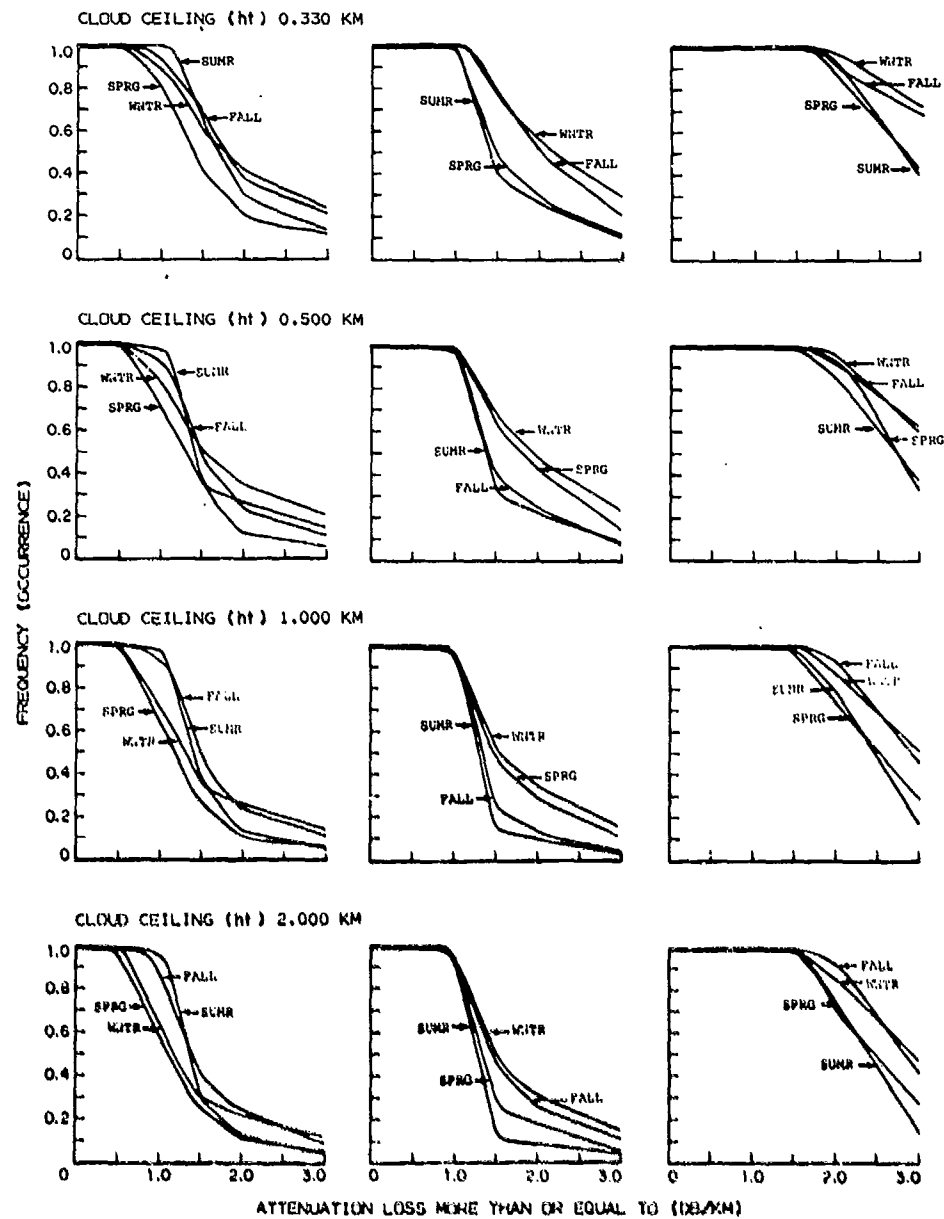


Fig. A 4.6 Joint Probability of Cloud Height and Clear Air/Fog-Haze Attenuation for IR Radiation Bands

HAMBURG, GERMANY
DAYTIME HOURS - 600 TO 1800 LST
FROM 1949 1 1 TO 1950 2 20

-5-6710

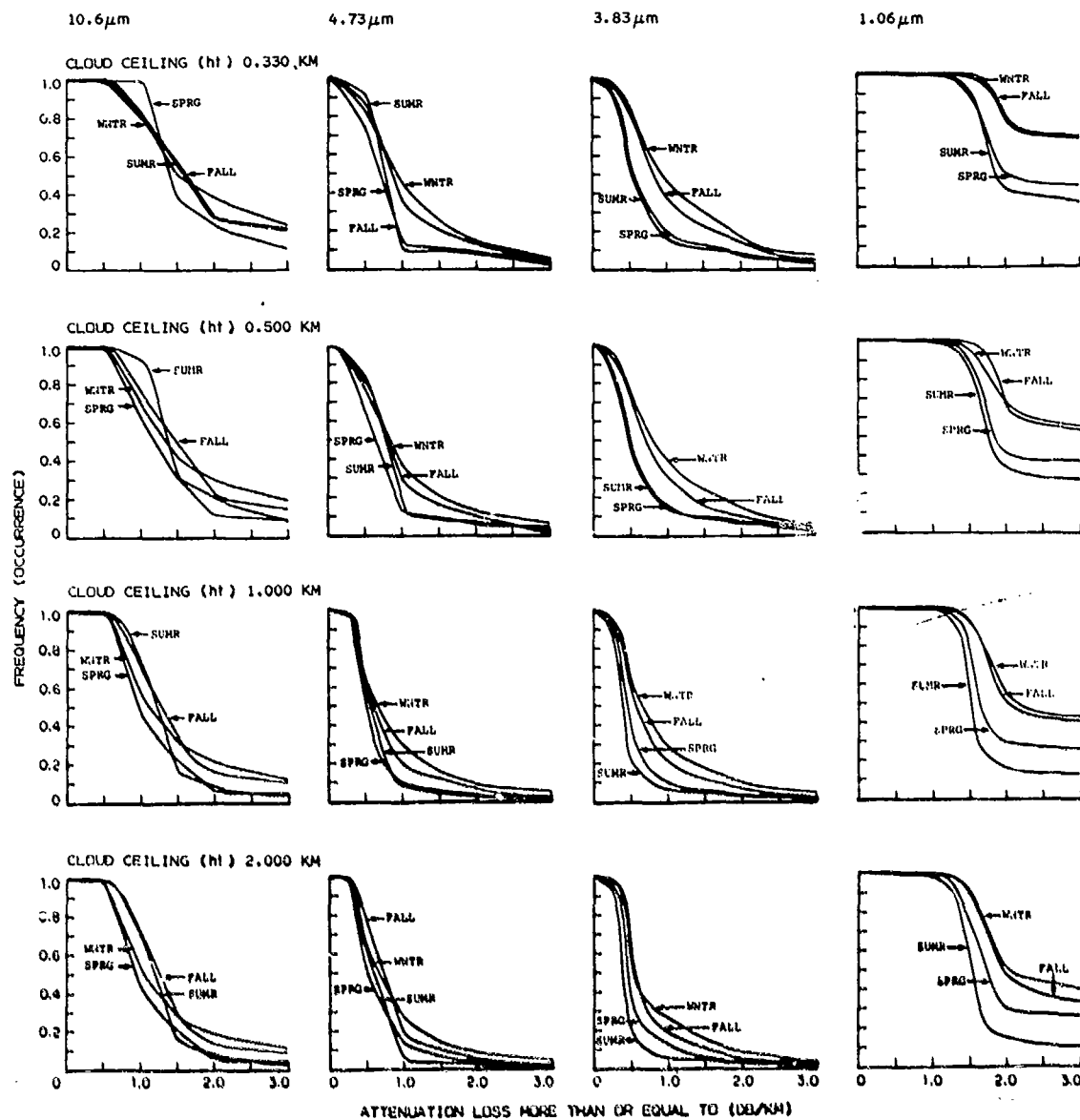


Fig. A 4.7 Joint Probability of Cloud Height and Clear Air/Fog-Haze Attenuation for Laser Lines

CAIRO, EGYPT
DAYTIME HOURS-600 TO 1800 LST
FROM 1957 1 1 TO 1963 5 25

TT-7 (A5.1)

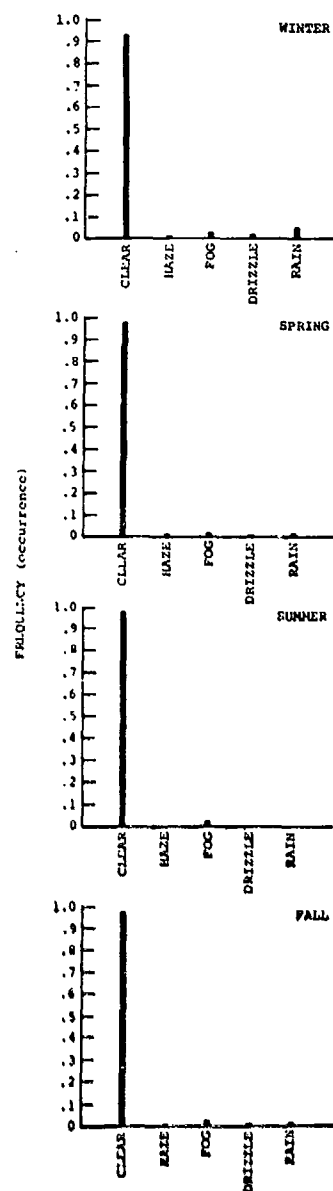


Fig. A 5.1 Probability of Synoptic Weather

TT-7 (A5,2)

CLOUD CEILING HEIGHT GREATER THAN 10KM FOR >.90
FREQUENCY OF OCCURRENCE ALL SEASONS.

Fig. A 5.2 Probability of Cloud Ceiling Height

TT-7 (A5.3)

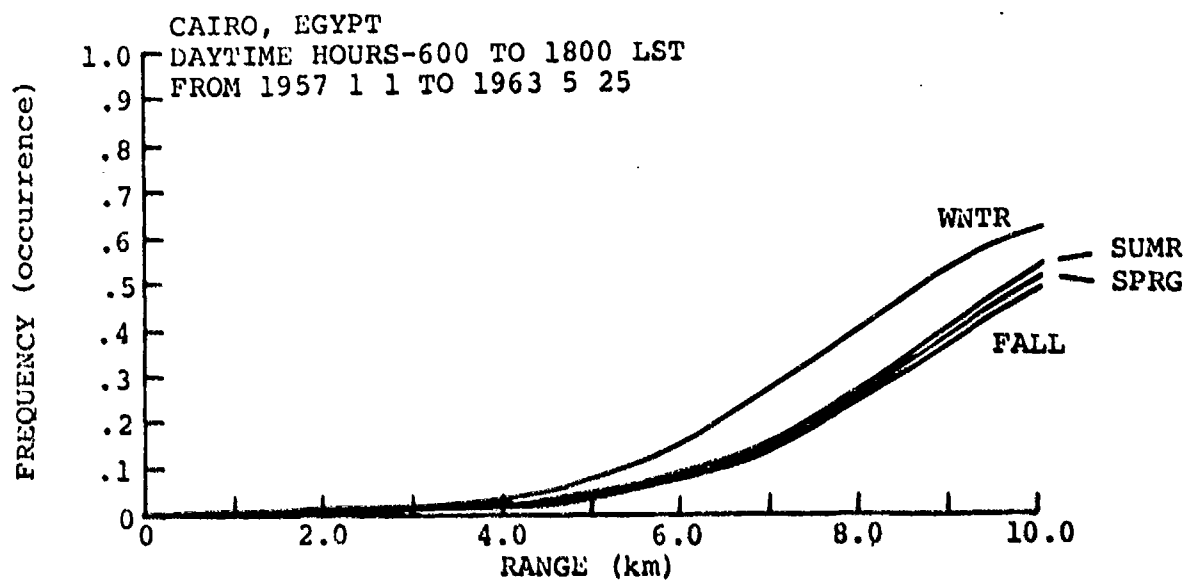


Fig. A 5.3 Probability of Photopic Visibilities

CAIRO EGYPT
DAYTIME HOURS-600 TO 1800 LST
FROM 1957 1 1 TO 1963 5 25

TT-7 (A5.4)

ATMOSPHERIC ATTENUATION:

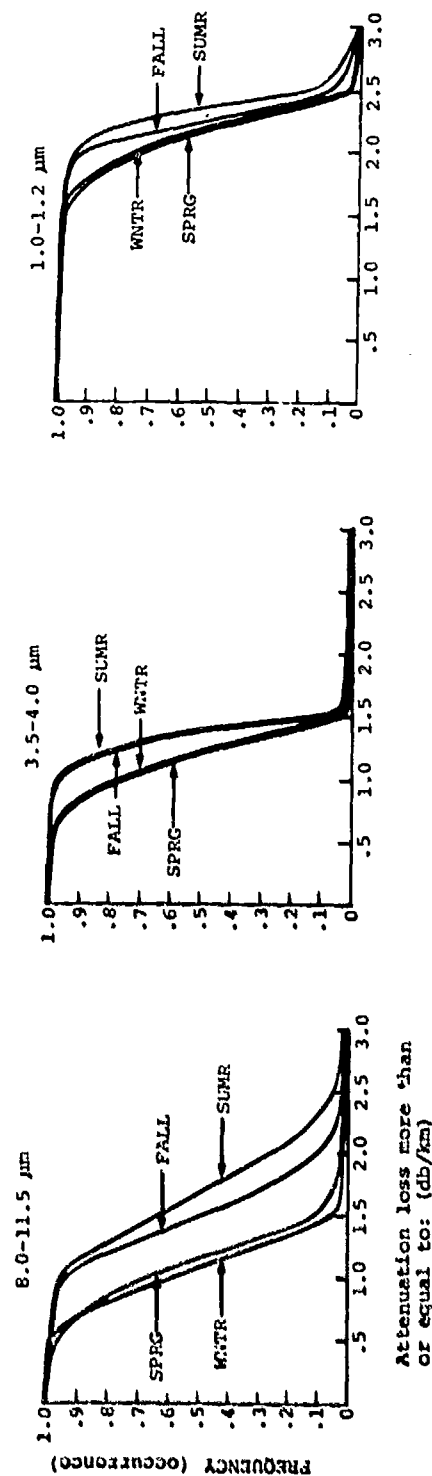


Fig. A 5.4 Probability of Clear Air/Fog-Haze Atmospheric Attenuation for IR Radiation Bands

CALCULATED
DAILY LOSS-400 TO 1420 LST
FROM 1957 1 1 TO 1963 5 25

ATMOSPHERIC ATTENUATION

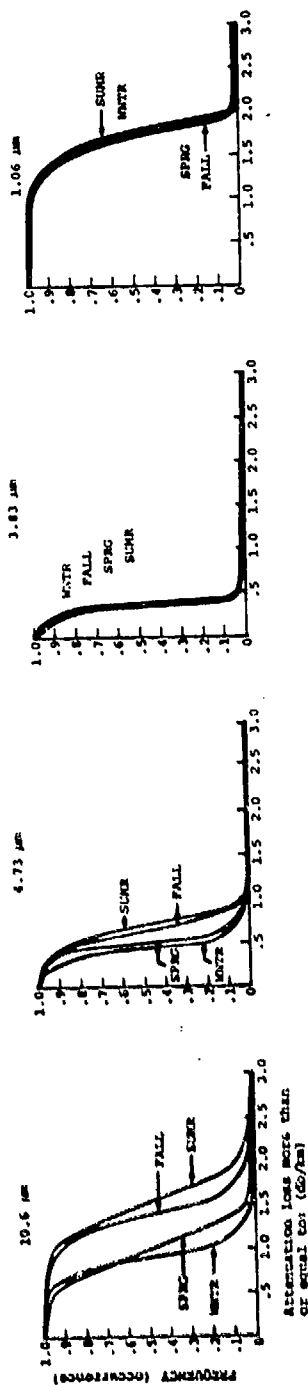


Fig. A 5.5 Probability of Clear Air/Fog-Haze Atmospheric Attenuation for Laser Lines

TT-7 (A5.5)

Joint meteorological data not available.

Fig. A 5.6 Joint Probability of Cloud Height and Clear Air/Fog-Haze
Attenuation for IR Radiation Bands

Joint meteorological data not available.

Fig. A 5.7 Joint Probability of Cloud Height and Clear Air/Fog-Haze
Attenuation for Laser Lines

TT-7 (A6.1)

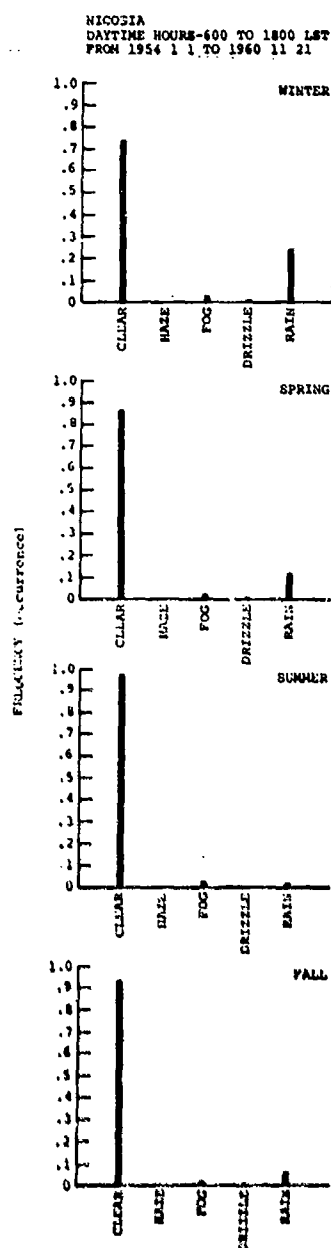


Fig. A 6.1 Probability of Synoptic Weather

TT-7 (A6.2)

NICOSIA
DAYTIME HOURS- 600 TO 1800 LST
FROM 1954 1 1 TO 1959 7 3

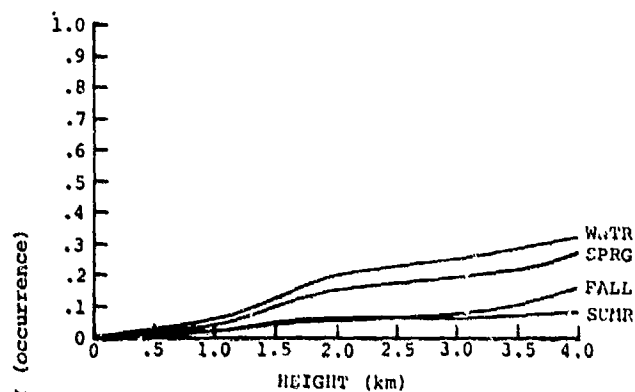


Fig. A 6.2 Probability of Cloud Ceiling Height

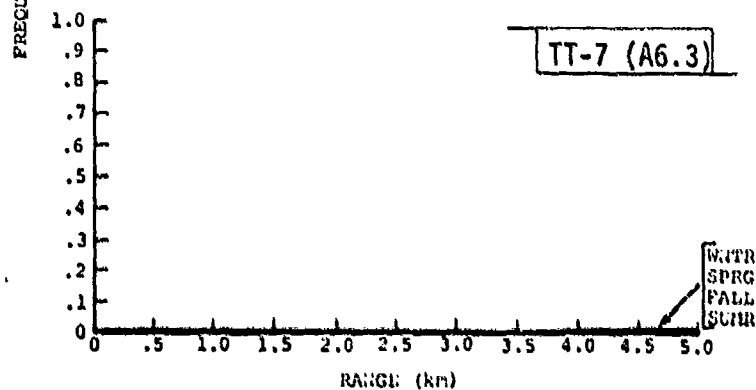


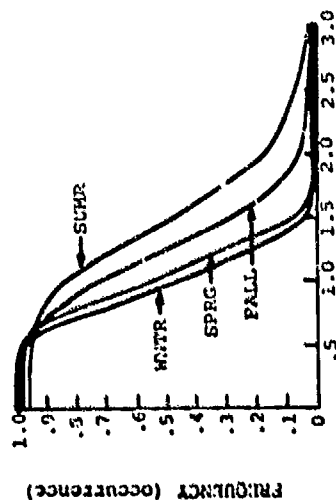
Fig. A 6.3 Probability of Photopic Visibilities

NICOSIA
DAYTIME HOURS-600 TO 1800 LST
FROM 1954 1 1 TO 1960 11 21

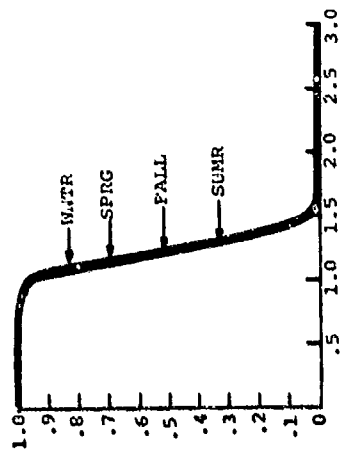
TT-7 (A6.4)

ATMOSPHERIC ATTENUATION

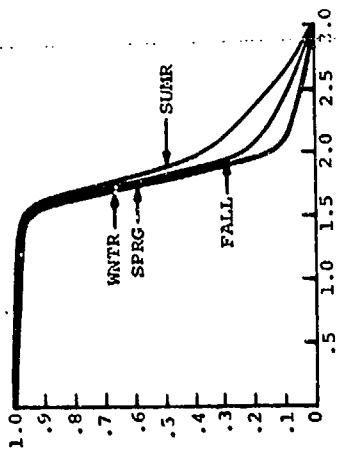
8.0-11.5 μm



3.8-4.2 μm



1.0-1.2 μm



Attenuation loss more than
or equal to: (db/km)

Fig. A 6.4 Probability of Clear Air/Fog-Haze Atmospheric Attenuation
for IR Radiation Bands

GEORGIA
WINTER-418-1818 LET
FROM 1916 1:1 TO 1965 1:1

ATTENUATION

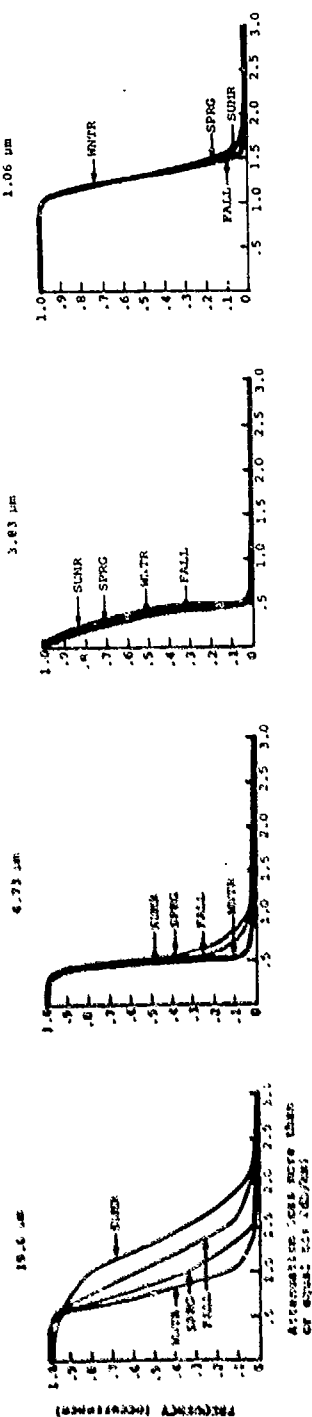


Fig. A 6.5 Probability of Clear Air/Fog-Haze Atmospheric Attenuation
for Laser Lines

TT-7 (A6.5)

NICOSIA
DAYTIME HOURS - 600 TO 1800 LST
FROM 1954 1 1 TO 1960 11 21

-5-6704

8.0 - 11.5 μm

3.8 - 4.2 μm

1.0 - 1.2 μm

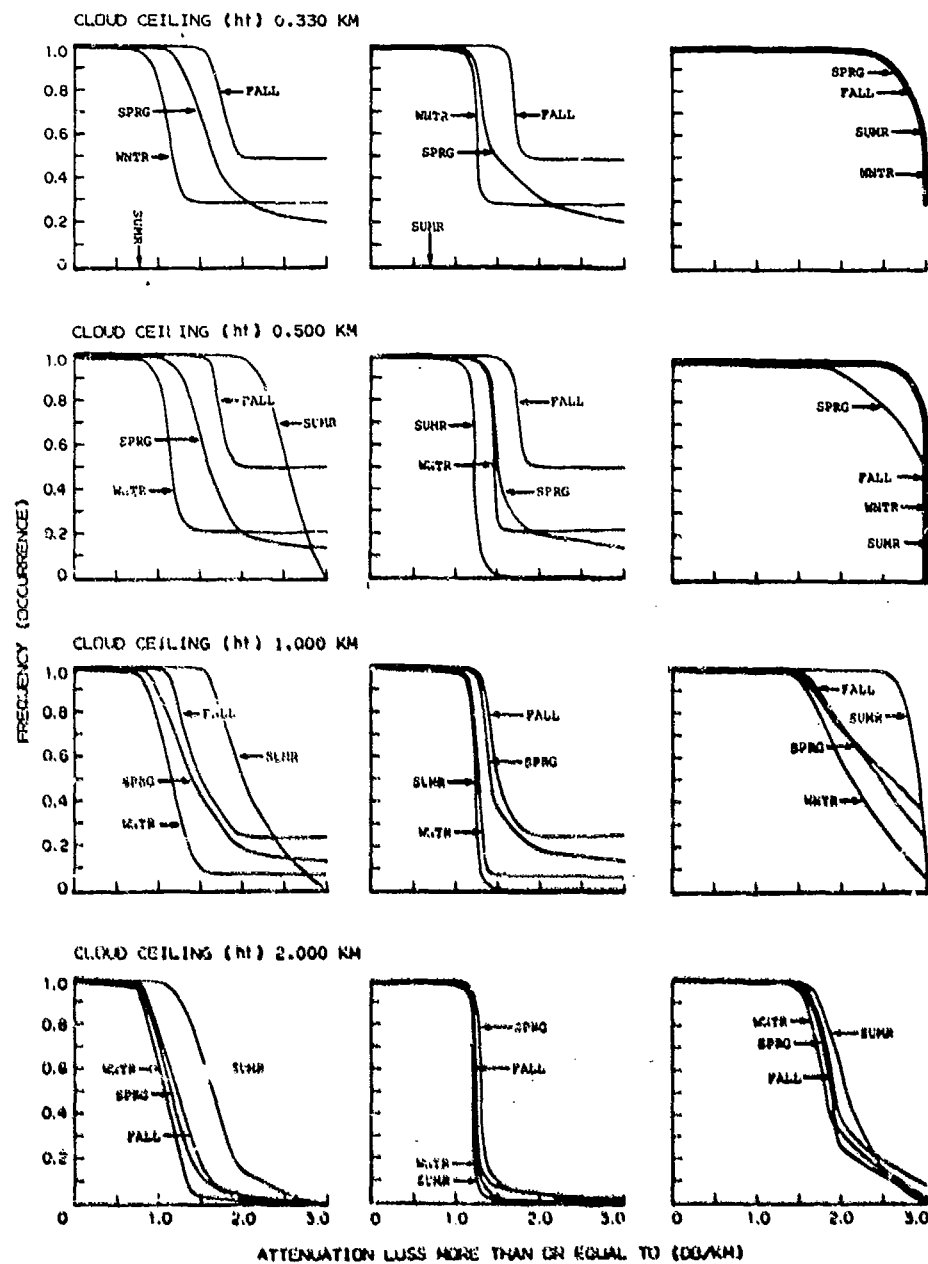


Fig. A 6.6 Joint Probability of Cloud Height and Clear Air/Fog-Haze Attenuation for IR Radiation Bands

NICOSIA
DAYTIME HOURS - 600 TO 1800 LST
FROM 1954 1 1 TO 1960 11 21

-5-6713

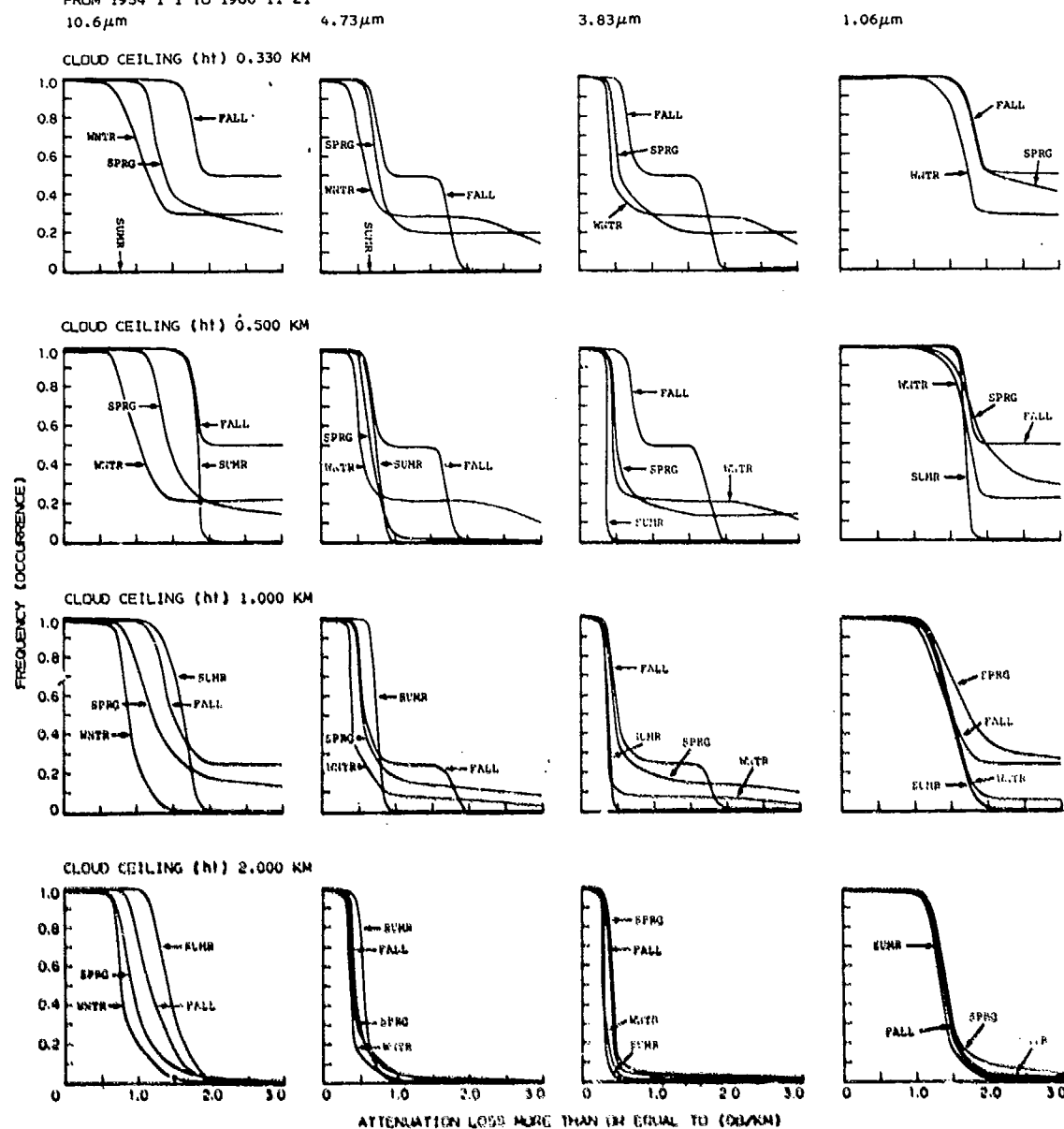


Fig. A 6.7 Joint Probability of Cloud Height and Clear Air/Fog-Haze Attenuation for Laser Lines

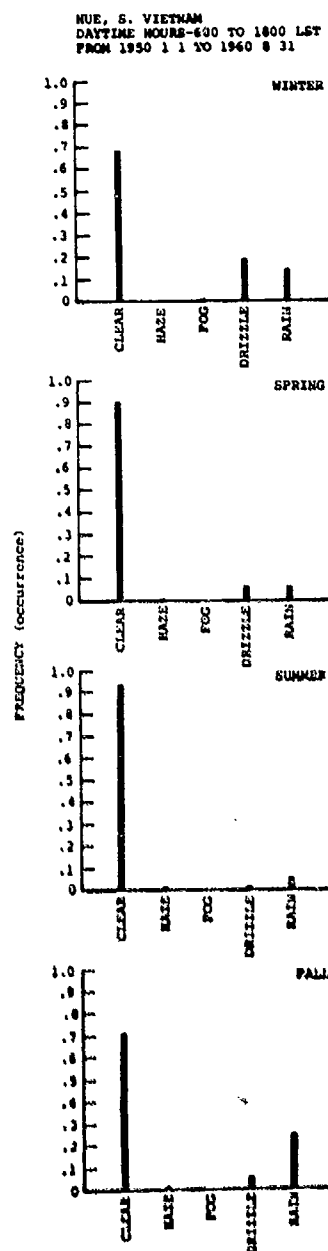


Fig. A 7.1 Probability of Synoptic Weather

HUE, S.VIETNAM
 DAYTIME HOURS-600 TO 1800 LST
 FROM 1950 1 1 TO 1958 9 21

TT-7 (A7.2)

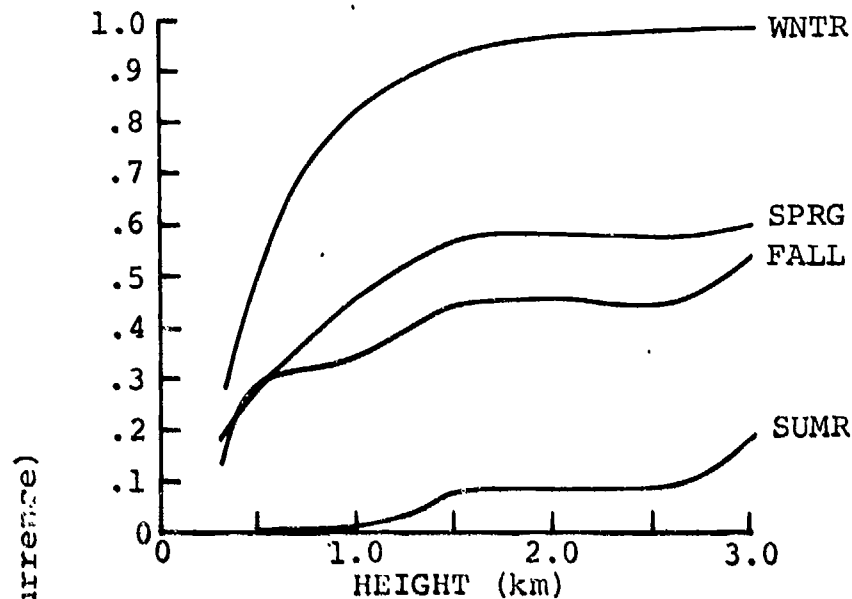


Fig. A 7.2 Probability of Cloud Ceiling Height

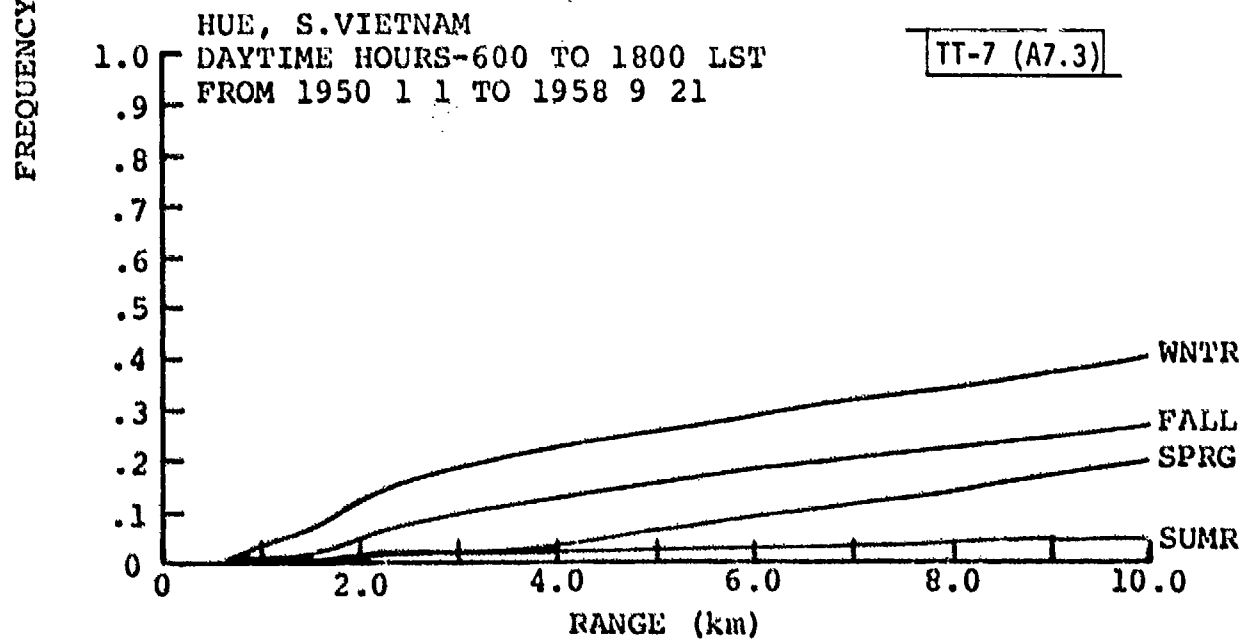


Fig. A 7.3 Probability of Photopic Visibilities

LEE, S. VILTIAM
DAYTIME HOURS-600 TO 1800 LST
FROM 1950 1 1 TO 1958 9 21

TI-7 (A7.4)

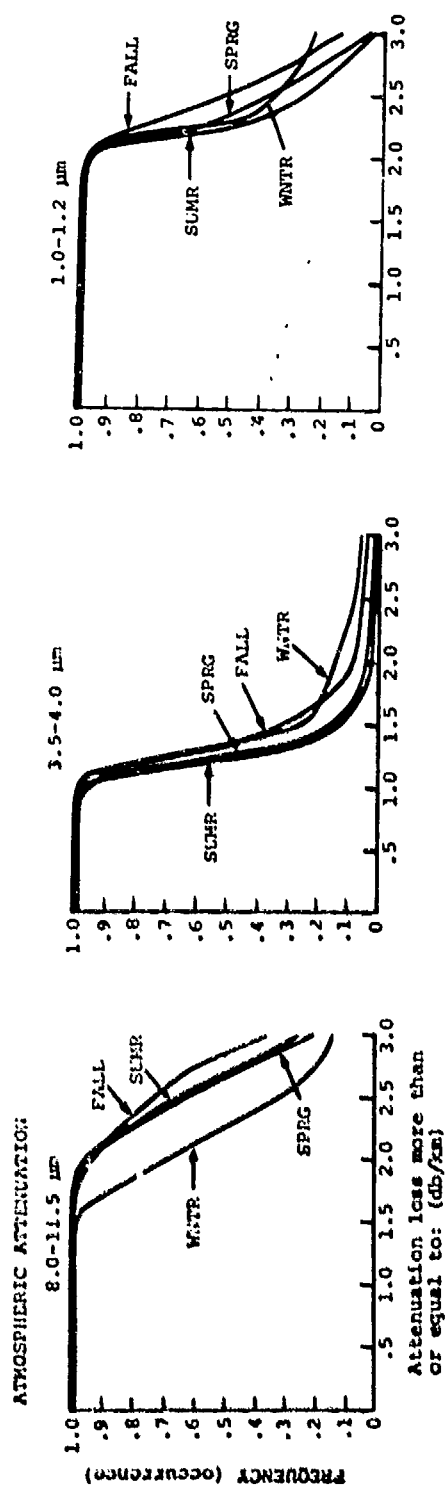


Fig. A 7.4 Probability of Clear Air/Fog-Haze Atmospheric Attenuation for IR Radiation Bands

REF. 5. VITKAMP
DAYTIME WOLVES-ACD TO 1800 MFT
FROM 1910 1 1 TO 1918 9 71
ATMOSPHERIC ATTENUATION.

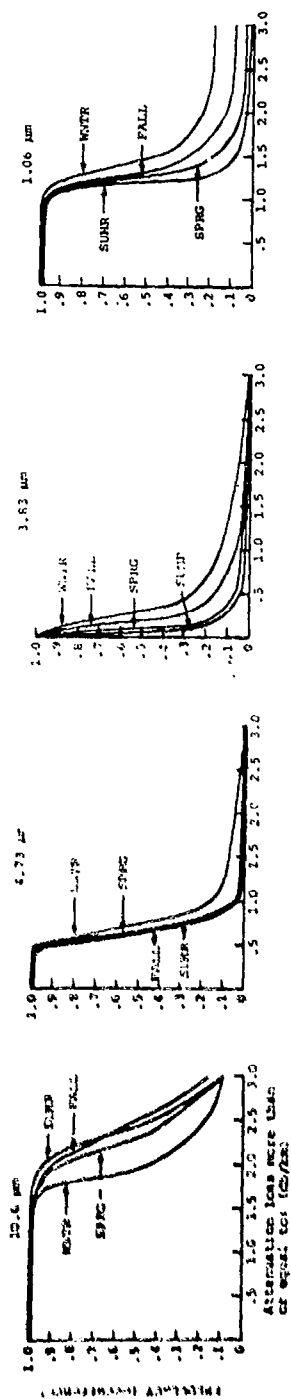


Fig. A 7.5 Probability of Clear Air/Fog-Haze Atmospheric Attenuation
for Laser Lines

TT-7 (A7.5)

Joint meteorological data not available.

Fig. A 7.6 Joint Probability of Cloud Height and Clear Air/Fog-Haze
Attenuation for IR Radiation Bands

Joint meteorological data not available.

Fig. A 7.7 Joint Probability of Cloud Height and Clear Air/Fog-Haze
Attenuation for Laser Lines

TT-7 (A8.1)

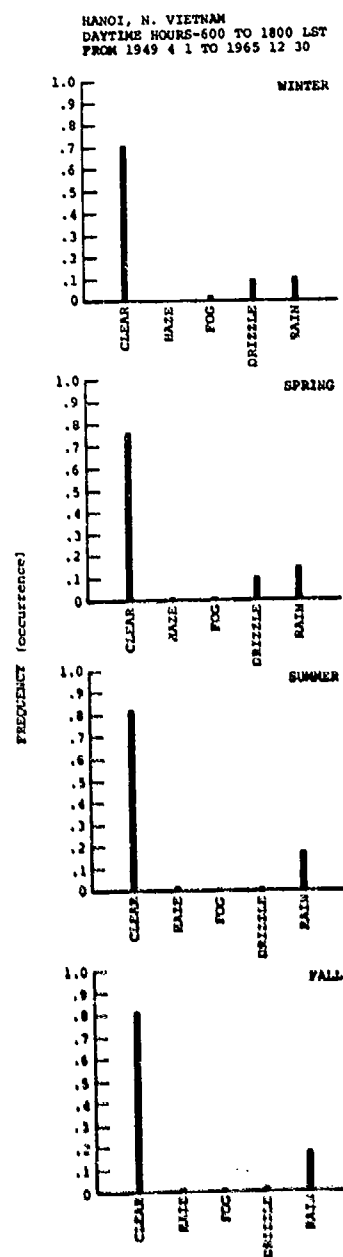


Fig. A 8.1 Probability of Synoptic Weather

Meteorological data not available.

Fig. A 8.2 Probability of Cloud Ceiling Height

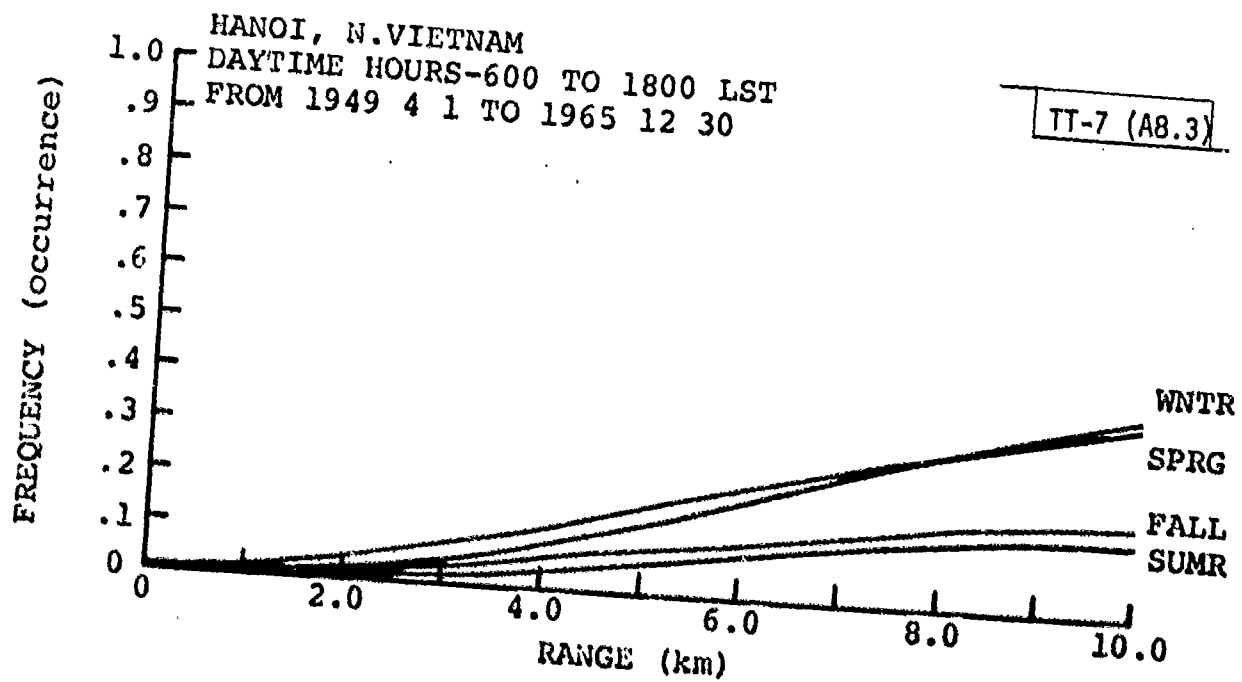


Fig. A 8.3 Probability of Photopic Visibilities

HAZARD, A. VILTAJ
DAYTIME HOURS-600 TO 1800 LST
FROM 1949 4 1 TO 1961 5 1

TT-7 (A8.4)

ATMOSPHERIC ATTENUATION
2.0-11.5 μ

3.5-4.7 μ

1.0-2.0 μ

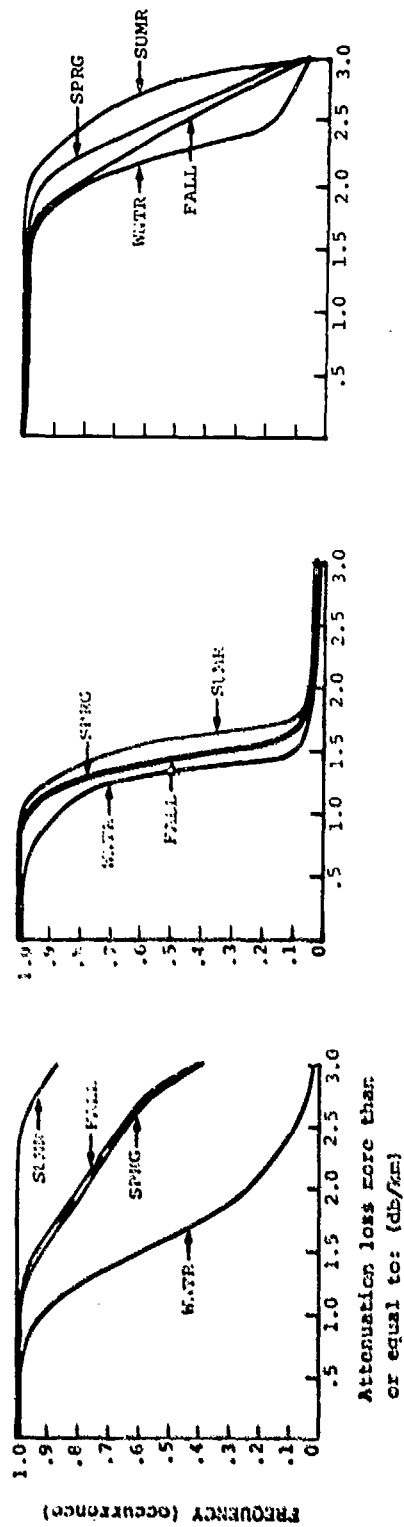


Fig. A 8.4 Probability of Clear Air/Fog-Haze Atmospheric Attenuation for IR Radiation Bands

RAMO, R. WILKINSON
DAYTIME MOIST-600 TO 1825 LF
FROM 1965 6 1 TO 1962 5 1

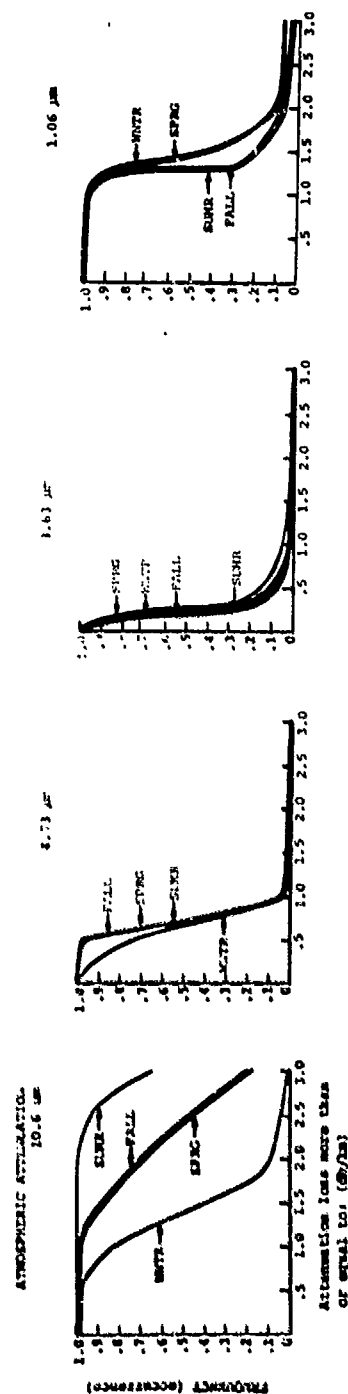


Fig. A 8.5 Probability of Clear Air/Fog-Haze Atmospheric Attenuation
for Laser Lines

Joint meteorological data not available.

Fig. A-8.6 Joint Probability of Cloud Height and Clear Air/Fog-Haze
Attenuation for IR Radiation Bands

Joint meteorological data not available.

Fig. A 8.7 Joint Probability of Cloud Height and Clear Air/Fog-Haze
Attenuation for Laser Lines

Meteorological data not available

Fig. A 9.1 Probability of Synoptic Weather

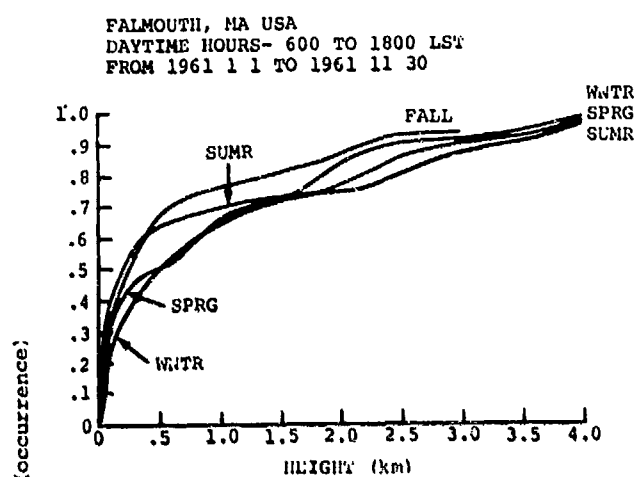


Fig. A 9.2 Probability of Cloud Ceiling Height

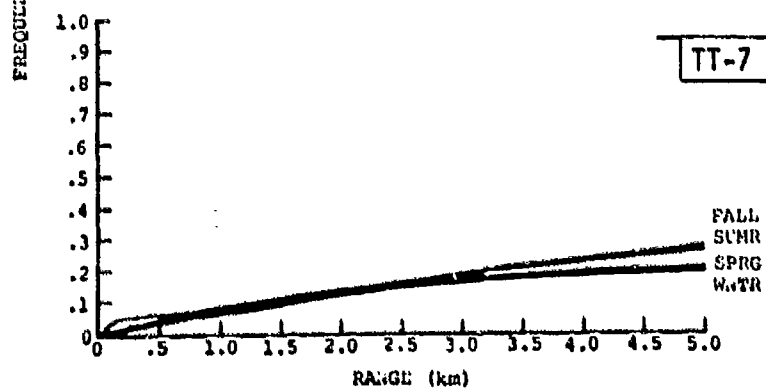


Fig. A 9.3 Probability of Photopic Visibilities

FALGOUTE PA USA
 DAYTIME HOURS-0800 TO 1800 EST
 FROM 1961 1 1 TO 1962 2 21

IT-7 (A9.4)

ATMOSPHERIC ATTENUATION

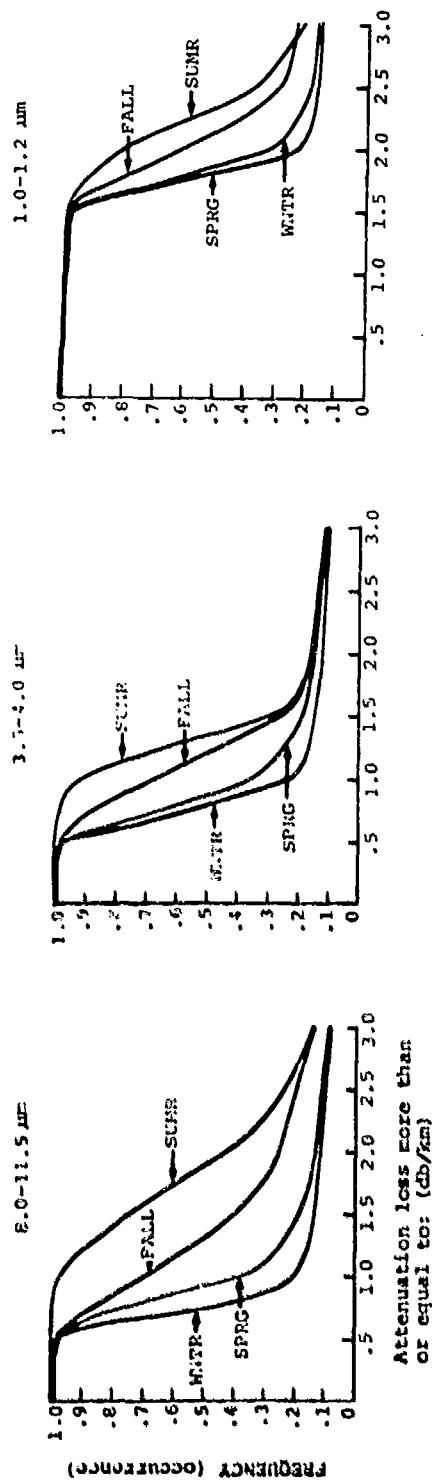
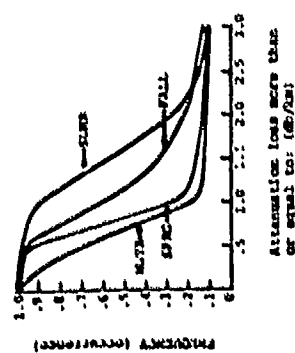


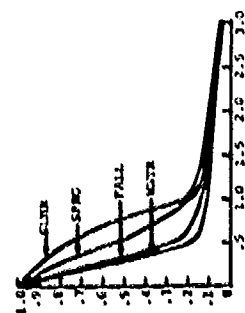
Fig. A 9.4 Probability of Clear Air/Fog-Haze Atmospheric Attenuation for IR Radiation Bands

FAUCONER ET AL
DAYTIME SOLAR-488 TO 1810 LST
FROM 1965 1 1 TO 2 21

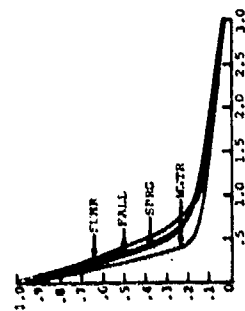
ATMOSPHERIC ATTENUATION
18.6 μ m



4.75 μ m



3.83 μ m



1.06 μ m

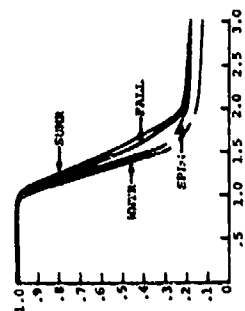


Fig. A 9.5 Probability of Clear Air/Fog-Haze Atmospheric Attenuation for Laser Lines

TT-7 (A9.5)

FALMOUTH MA, USA
 DAYTIME HOURS - 600 TO 1800 LST
 FROM 1961 1 1 TO 1962 2 21
 8.0 - 11.5 μm

-A-8707

3.8 - 4.2 μm

1.0 - 1.2 μm

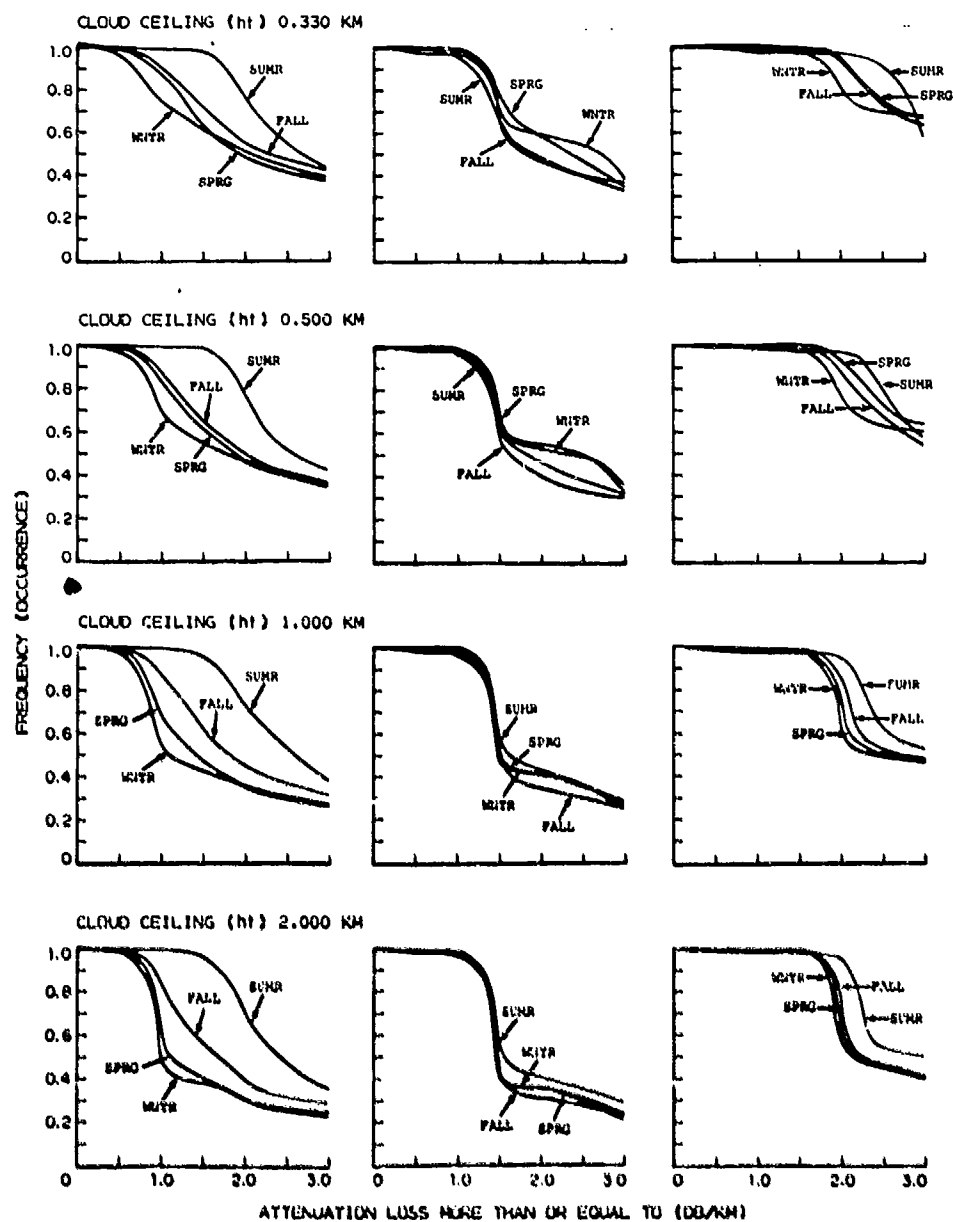


Fig. A 9.6 Joint Probability of Cloud Height and Clear Air/Fog-Haze Attenuation for IR Radiation Bands

FALMOUTH, MA. USA
DAYTIME HOURS - 600 TO 1800 LST
FROM 1961 1 1 TO 1962 2 21

-5-8708

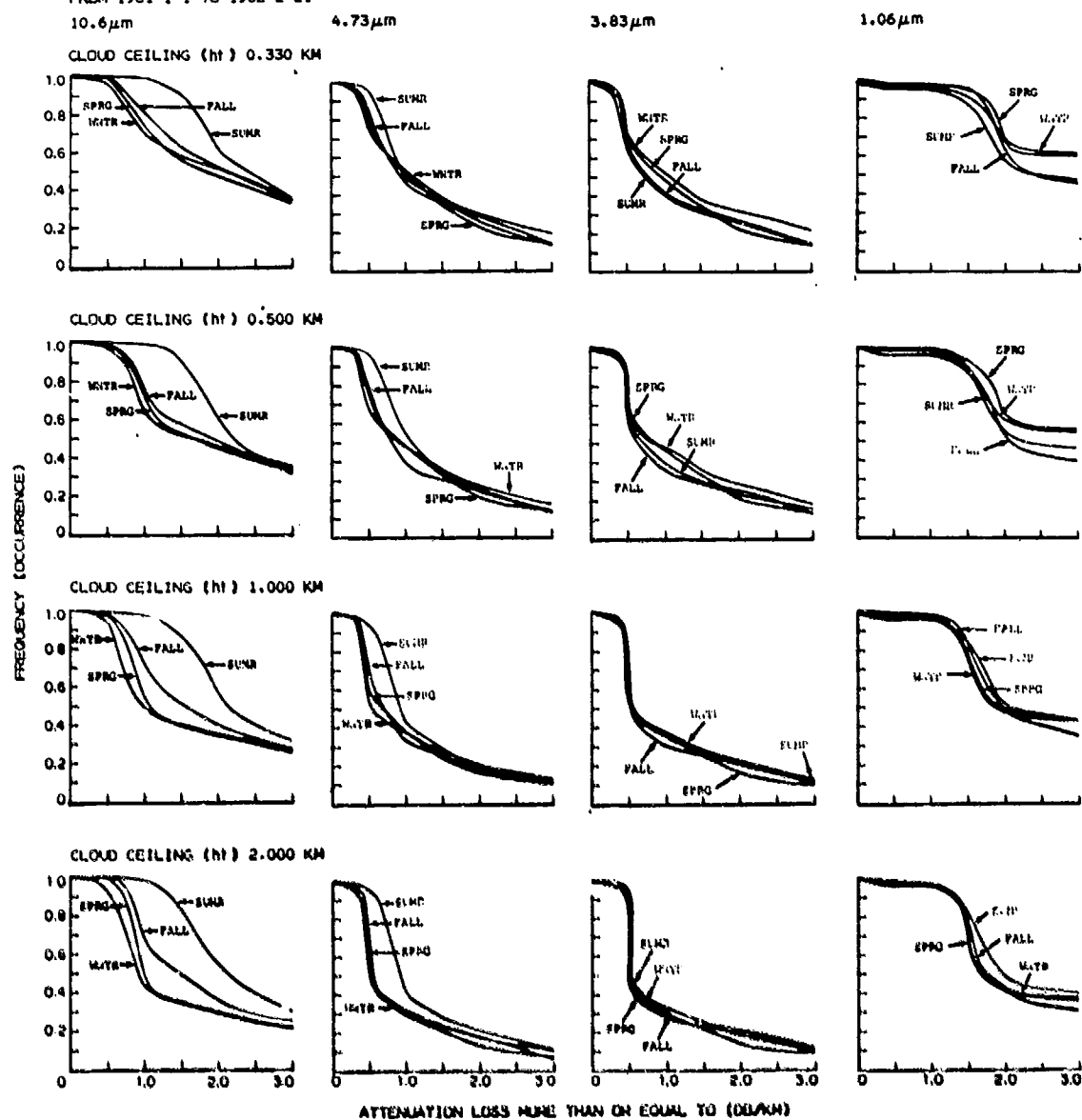


Fig. A 9.7 Joint Probability of Cloud Height and Clear Air/Fog-Haze Attenuation for Laser Lines

UNCLASSIFIED

SECURITY CLASSIFICATION OF THIS PAGE (When Data Entered)

REPORT DOCUMENTATION PAGE		READ INSTRUCTIONS BEFORE COMPLETING FORM	
1. REPORT NUMBER ESD-TR-76-67	2. GOVT ACCESSION NO.	3. RECIPIENT'S CATALOG NUMBER	
4. TITLE (and Subtitle) Statistics of Global IR Atmospheric Transmission	5. TYPE OF REPORT & PERIOD COVERED Project Report		
7. AUTHOR(s) Anthony P. Modica and Herbert Kleiman	6. PERFORMING ORG. REPORT NUMBER Project Report TT-7		
9. PERFORMING ORGANIZATION NAME AND ADDRESS Lincoln Laboratory, M.I.T. P.O. Box 73 Lexington, MA 02173	8. CONTRACT OR GRANT NUMBER(s) F19628-76-C-0002 ARPA Order-2752		
11. CONTROLLING OFFICE NAME AND ADDRESS Defense Advanced Research Projects Agency 1400 Wilson Boulevard Arlington, VA 22209	10. PROGRAM ELEMENT, PROJECT, TASK AREA & WORK UNIT NUMBERS ARPA Order 2752 Program Element No. 0610 Project No. 62702E		
14. MONITORING AGENCY NAME & ADDRESS (if different from Controlling Office) Electronic Systems Division Hanscom AFB Bedford, MA 01731	12. REPORT DATE 3 March 1976		
	13. NUMBER OF PAGES 102		
	15. SECURITY CLASS. (of this report) Unclassified		
16. DISTRIBUTION STATEMENT (of this Report) Approved for public release; distribution unlimited.			
17. DISTRIBUTION STATEMENT (of the abstract entered in Block 20, if different from Report)			
18. SUPPLEMENTARY NOTES None			
19. KEY WORDS (Continue on reverse side if necessary and identify by block number) <div style="display: flex; justify-content: space-between;"> <div>weather statistics atmospheric attenuation narrow IR bands</div> <div>transmission losses LOWTRAN HOWLS Program</div> <div>Project OPAQUE electro-optical systems</div> </div>			
20. ABSTRACT (Continue on reverse side if necessary and identify by block number) <p>RAND weather data tapes have been used to obtain statistics of visibility, relative humidity and cloud ceiling heights for weather stations throughout the Northern Hemisphere to generate global probabilities for atmospheric attenuation in the infrared spectral region. The present analysis predicts seasonal probabilities for horizontal sea level transmission losses for several narrow IR bands (1.0-1.2), (3.8-4.2), (8.0-11.5 μm) and four laser lines (1.06), (3.83), (4.73) and (10.6 μm). The results also include cloud-free line-of-sight probabilities and attenuation losses through rain.</p>			

DD FORM 1473 EDITION OF 1 NOV 65 IS OBSOLETE

UNCLASSIFIED

SECURITY CLASSIFICATION OF THIS PAGE (When Data Entered)

219650